Memoirs of the Faculty of Engineering, Nagoya University
Vol. 31, No. 2. (1979)

NONLINEAR INTERACTION OF HIGH FREQUENCY ELECTROMAGNETIC FIELD WITH A PLASMA

Hidenori AKIYAMA and Susumu TAKEDA

Department of Electrical Engineering

(Received November 2, 1979)

Abstract

The studies on the linear and nonlinear interactions between the electromagnetic waves and plasmas are of importance in order to understand the basic processes in the laser-pellet interaction, heating of magnetically confined plasma, and ionospheric modification.

In the present thesis are described the nonlinear interactions associated with the parametric and modulational instabilities, and ponderomotive force. The high frequency electromagnetic field inside a resonant cavity is applied to the quiescent plasma, which is produced by the Lisitano coil at the electron cyclotron resonance. The experimental conditions, where each nonlinear phenomenon is dominant, are obtained by adjusting the pump and electron plasma frequencies.

After the parametric decay of one pump field into the Langmuir and ion acoustic waves is studied, the double resonance parametric instability is experimentally confirmed for two pump fields, which have the frequency difference of twice the ion acoustic wave frequency. The modulational instability of the electron plasma wave is studied, comparing the experimental results with a theory. It is based on the coupling of the nonlinear schrödinger equation with the equation of the ion acoustic wave including the ponderomotive force. An experiment, in which the ponderomotive force is dominant, is carried out by using the electromagnetic wave with the higher frequency than the electron plasma frequency. The results obtained to confirm the ponderomotive force are extended to the experiments for suppressing the end loss of the mirror-confined plasma, and stabilizing the drift-cyclotron loss-cone instability.

CONTENTS

1. Introduction

1. 1. Historical Survey

The interactions between the electromagnetic waves and plasmas have been studied since a long time ago. Among them the linear dispersion relation has been already summarized in many books,[1~5] where the effects of static magnetic field, electron and ion temperatures, boundary, the collisions and nonuniformity of the mediums are theoretically Analyzed. Moreover, the dispersion characteristics of the electromagnetic wave propagating in the plasmas are utilized for the diagnosis of plasmas.[6]

The nonlinear interactions between the electromagnetic waves and plasmas have developed since about ten years ago, in connection with the heating of plasmas in magnetic traps, the study of the laser-pellet interaction and the modification of the ionosphere by a intense radar waves. The developed nonlinear phenomena mainly consist of the wave-wave and wave-particle nonlinear interactions and the coherent nonlinear wave propagation.

The parametric instability produced by the wave-wave interaction has been studied in unmagnetized plasmas by the many investigators.[7~51] This instability introduced from the dynamics to the plasma physics by Silin[7] can occur when the pump wave resonantly drives two waves, which satisfy the matching condition of the frequency and wavenumber. After this work, the extentions of the theory have been reported.[8~39] For example, DuBois and Goldman[8, 9] deduced the threshold for the parametric decay coupling of the electron plasma wave with ion acoustic one, where the Landau damping was considered. Jackson[10] studied the instability by the intense pump field on the basis of the Vlasov equation. And Nishikawa[11] predicted the oscillating two stream instability produced by the pump field with the lower frequency than the cut-off one. Perkins and Flick[21] showed an increase of the threshold by considering the inhomogeneity of the plasma density. Arnush et al.[31] predicted that the threshold power could be decreased when two pump fields whose frequency difference was equal or twice the ion acoustic frequency were applied. This phenomenon is called the double resonance parametric instability. Moreover, the saturation mechanisms, such as the nonlinear Landau damping, mode coupling and cascade process, are considered.[34~39]

The first observation of the parametric instability was carried out in a weakly-ionized and unmagnetized plasma immersed in a S-band waveguide by Stern and Tzoar,[40] who observed the frequency spectra of the decayed waves. After this report, many experiments[41~51] have been carried out using the waveguide, the cavity, the grid and horn to supply the electromagnetic wave to the plasma. For example, Dreicer et al.[41] demonstrated that the reduction in the quality factor Q of the resonant cavity occured at a certain pump power, which was presumed to be the threshold of the parametric instability. Afterwards Hendel and Flick[42] observed the ion and electron heatings due to the decayed wave, where the plasma was produced by Q-machine. Eubank[43] observed an increase of the threshold for the inhomogeneous plasma, where the open-ended waveguide was used to supply the pump power to the high density plasma. Stenzel and Wong[44] observed the double resonance parametric instability using two pump fields having a frequency difference equal to the ion acoustic wave frequency. The experiment[45] using a pump power higher than the threshold value was also reported for the purpose of studying nonlinear saturation and evolution. Moreover, the parametric instabilities in magnetized plasmas have been studied in relation to the heating of magnetically confined plasma.[52~61]

The modulational instability[62~73] as one of the coherent nonlinear wave phenomena has been theoretically described by the nonlinear Schrödinger equation, which was derived by Taniuti and Yajima[62] by means of the reductive perturbation method expanded to the third order. Asano et al.[66] reported that the electron plasma wave was stable for the modulational instability in an unmagnetized plasma with the cold ions. However, Zakharov[70] insisted that the electron plasma waves became unstable in a small wave number region, when the equation for the ion aco ustic wave including the ponderomotive force term is coupled with the nonlinear Schrödinger equation. Nishikawa et al.[71] obtained the solitary wave solutions as a special case by analyzing both the nonlinear Schrödinger equation and Korteweg-de Vries equation modified so as to include the ponderomotive force.

Some experiments[74~79] in relation to the modulational instability have been reported. Kim et al.[74] and Ikezi et al.[75] independently observed the enhancement of the high frequency electric field trapped by the density depression, and the obtained results were explained by Nishikawa et al.[71] Then Wong and Quon[77] observed that the electron plasma wave excited by the electron beam collapsed into the intense field spikes. This might be a developed state of the modulational instability described by Zakharov.[70] Then some computer simulations were also reported.[80~83]

The ponderomotive force,[84~86] which changes the density profile of the plasma, is important as a basic process of some nonlinear phenomena. Veksler[87] proposed to confine the plasma using a high frequency field. Following such suggestion, the theories[88~95] and experiments[96~103] have been reported by many investigators. Sato et al.[98] succeeded to decrease the plasma loss from the cusp magnetic field using the elctromagnetic field near the ion cyclotron resonance. Dougar-Jabon et al.[102] observed the suppression of end loss from the mirror magnetic field using a cavity resonating at the electron cyclotron frequency. Shelby and Hatch[103] tried the plasma confinement in the resonant cavity by the ponderomotive force without the magnetic field.

Lastly, the drift-cyclotron loss-cone (DCLC) instability and its suppression will be described. This instability[104, 105] restricts the confinement time of the

plasma in the mirror magnetic field as shown by the experiment on 2X ⅡB device[114] at Lawrence Livermore Laboratory. Post and Rosenbluth[106] analyzed theoretically DCLC instability with the Cartesian co-ordinate, and Shima and Fowler[107] did with the cylindrical co-ordinate. The saturation mechanism and the finite β effect were also studied.[108~113] The instability can be stabilized by controling the radial density and particle velocity distribution of the driving force. For example Coensgen et al.[114] used the cold plasma stream to modify the loss-cone velocity distribution. Logan et al.[115] modified the distribution by the low energy plasma, which was produced by ionizing the neutral particles in the gas box located at the mirror end. Kanaev et al.[116] stabilized DCLC instability by the low energy ions trapped in the potential well produced by the microwave. There is another proposal[117] such as the trapping of low energy particles in the potential well produced by the tailored magnetic field.

1. 2. Purpose and Scope of the Present Work

Research on nonlinear interactions between the electromagnetic wave and plasma has been developed remarkably along with the investigations of the laser-pellet interaction and heating of the collisionless plasma. The observation of the nonlinear phenomena by laser is difficult, and the measured plasma parameters are restricted, since the phenomena occur in the extremely fast time and small spatial scales. The similar phenomena can be observed in detail using the microwave instead of laser, since the phenomena develop with the slower temporal and larger spatial scales than those of the laser-plasma interactions.

The present series of works have started with the purpose to investigate some nonlinear interactions between the microwave and plasma. A plasma with a density of $10^9 \sim 10^{11}$ cm^{-3} produced by the Lisitano coil[118, 119] is appropriate for the experiments of the wave and instability, because the density fluctuation is the low level. The microwave field is supplied to the plasma by a resonant cavity operating at TM_{010} mode. Then a sufficiently high intensity field can be easily obtained with a relatively small input power to the cavity. Moreover, the plasma density and effective collision frequency can be known by measuring the resonant frequency of the cavity and quality factor respectively.

In chapter 2, the decay instability is studied by using the electromagnetic wave with the frequency near the electron plasma frequency. Dreicer et al.[41] first demonstrated only that the effective collision frequency increased when the microwave power feeding the cavity which contained c_s plasma of Q-machine exceeded a threshold value. In order to identify the type of the decay instability still more, we made measurement of the frequency spectra and wave numbers of the induced ion acoustic and electron plasma waves, and observed an increase of the electron temperature in addition to the measurement of the effective collision frequency. Moreover, we found that the amplification of the high frequency electric field and the decrease of the density occured at the cut-off region, which existed in the nonuniform plasma. These phenomena were explained by the theories of white et al.[120] and the ponderomotive force.

In chapter 3, the double resonance parametric instability predicted by Arnush et al.[31] is confirmed experimentally. Stenzel and Wong[44] reported that the waves excited by two pump fields with the frequency difference equal to the ion acoustic wave frequency had the larger amplitude than those excited by one pump field. We study the double resonance parametric process by using the two

pump fields with the frequency difference, which is twice the ion acoustic wave frequency, and the experimental results are compared with the theory.[31]

The experiments on the modulational instability of the electron plasma wave are reported by Wong and Quon.[77] However, no direct comparison between the experiment and theory is possible, since the amplitude of the electron plasma wave in such well-developed situation is too large. Therefore in chapter 4, the modulational instability of the electron plasma wave with the small amplitude is studied following the comparison with the theory, which is derived from the basic equation used by Zakharov.[70] This phenomenon is related not only to the laser-pellet interaction but also to the heating of the plasma by the relativistic electron beam.

The nonlinear interactions between the electromagnetic wave and plasma, such as the oscillating two stream instability,[11] resonant absorption,[120] are mainly caused by the ponderomotive force. The experiment, in which only the ponderomotive force is relevant factor, is important for the full understanding of the nonlinear phenomena. Therefore in chapter 5, an experiment on the ponderomotive force is carried out using an intense high frequency field in the resonant cavity. The frequency of the electromagnetic wave used is selected to be higher than the electron plasma frequency to prevent other nonlinear phenomena.

In chapter 6, the results obtained in chapter 5 are utilized to suppress the end loss of the mirror-confined plasma. The electromagnetic waves with the electron and ion cyclotron frequencies are generally used to suppress the plasma loss from the mirror[102] and cusp[98] magnetic fields respectively. However, the suppression mechanism is not quantitatively so clear, since the effects of both the plasma confinement and heating caused by the cyclotron resonance are not considered in the theory.[121] The adiabatic plugging is here studied using the electromagnetic wave near the electron plasma frequency and off the cyclotron resonance. Then the obtained results can be compared with a theory which takes into accounts the mirror effect and ponderomotive force.

In chapter 7, the identification and suppression of DCLC instability are studied. The frequency and the direction of propagation of DCLC instability were measured in 2X Ⅱ device at the Lawrence Livermore Laboratory.[104] In order to identify the instability more clearly, we measure the wave number and spatial localization in addition to the measurement of the frequency and the direction of propagation. The obtained dispersion relation is consistent with the theory.[106] The DCLC instability is next suppressed by the ponderomotive force, which changes the loss-cone velocity distribution to the loss-hyperboloid one. This method is a new one to stabilize the DCLC instability.

2. Parametric Instability and Electric Field Amplification in a Nonuniform Plasma

2. 1. Introduction

Since the theoretical analysis of the parametric excitation of the coupled waves have been published,[7, 8, 10, 11, 19, 21] meny experimental[40, 41, 49, 51, 122, 123] and computer simulated[124~126] results are reported. Dreicer et al.[41] first demonstrated that the effective collision frequency increased when a microwave power to a cavity which contained a C_s plasma of Q-machine exceeded a threshold value. They

attributed the effect to the parametric decay of the high frequency electric field into the Langmuir and ion acoustic waves by showing that the threshold value coincided with the theoretically predicted one. It should be emphasized, however, that the parametrically excited low and high frequency waves are neither observed nor identified in their experiment.

The increase of the electron temperature T_e and decrease of the density N at $\omega_0 \cong \omega_{pe}$ in a highly ionized plasma were found by Minami et al.[127] using a pulsed microwave, where ω_0 and ω_{pe} are respectively the applied pump and plasma frequencies. Ikezi et al.[75] observed the localized field and density depressions, and also observed their propagation parallel to the density gradient. Sugai et al.[128] observed a large amplitude ion wave excited by the ponderomotive force of electromagnetic wave. Our experiment is different from their ones in that the polarization of the electromagnetic field is perpendicular to the density gradient and that the observation is performed in a steady state.

In the present chapter, we describe the details of the parametric processes in the Lisitano plasma,[118] where the electron temperature T_e is much higher than the ion temperature T_i. This condition is suitable to excite ion acoustic waves, in contrast to Q-machine where the excited waves would be strongly Landau damped. The parametric decay of high frequency electric field into the Langmuir and ion acoustic waves appears for $\omega_0 > \omega_{pe}$ as expected. It is also found that the effective collision frequency ν_{eff} has two distinct breaking points as a function of the high frequency field intensity. When the field intensity is greater than the first breaking point, the frequency spectrum of ω_0 is only broadened, while the low frequency spectrum does not change. Above the second point for the higher input power, the excited low and high frequencies are observed on the spectrum analyser.

The dependence of the density depression on the amplified electric field of the frequency of ω_0 is also investigated with a reasonable agreement between the experimental result and theory. The mechanism is explained in terms of the ponderomotive force of the high frequency field induced along the density gradient, as expected by theory.[84]

In 2. 2 is described the experimental apparatus. In 2. 4, the experimental results written in 2. 3 are discussed in comparison with the theory. The results obtained are summarized in 2. 5.

2. 2. Experimental Apparatus

The schematic diagram is shown in Fig. 2. 1. The plasma is produced by the Lisitano coil[118] to which the microwave power is supplied from a cw magnetron operating at a frequency of 2450 MHz with maximum output power 500 watt. Lisitano coil with a diameter of 38 mm has the 12 slits each having 2 mm in width and 60 mm in length. The magnetic field of 875 gauss is applied to the Lisitano coil to meet the condition of electron cyclotron resonance. The resonance point is located inside the Lisitano coil. By adjusting

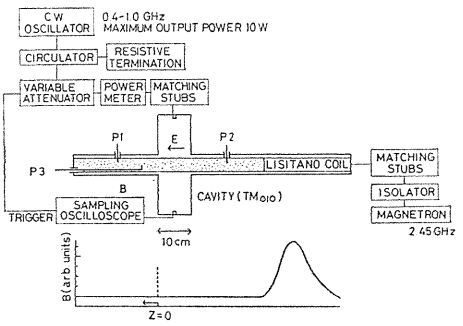

Fig. 2. 1. Schematic diagram.

the position of the solenoid coil and its exciting current, the best condition is obtained for producing a stable plasma with a proper density. Then the plasma expands in the axial direction with an almost constant diameter of about 4 cm.

Output power of a few watts from the cw oscillator with the variable frequency is fed to the loop antenna inside the cavity through the circulator, variable attenuator, power meter and matching stubs. The cavity has the diameter of 30 cm, the length of 10 cm, Q-value of 1400 and resonant frequency of 763 MHz without the plasma. No glass tube is used in order to eliminate the dielectric loss in the cavity. The high frequency electric field inside the cavity is parallel to the plasma axis and the static magnetic field, and has only the mode TM_{010}, because the skin depth of the electric field inside the plasma is much longer than the plasma diameter. Then the static magnetic field, which is almost parallel to the axis for sustaining the plasma steadily, does not interact with the high frequency field. The output signal, which is picked up by another loop antenna, is fed to the sampling oscilloscope. It can display the original wave form of high frequency signal without using the crystal detector.

The Langmuir probes P 1 and P 2 with diameter of 1 mm are radially movable, and probe p 3 of same dimension is axially movable. These probes are used to measure the electron temperature, density, and the fluctuation in the plasma. The ion temperature is measured by the multi-gridded probe of the diameter of 5 mm with two mesh grids. Either P 1 or P 2 is replaced by this probe when T_i is being measured.

Argon gas is used with a pressure of 10^{-4} Torr. The electron temperature T_e is a few eV, the ion temperature T_i divided by T_e is about 0.3, the plasma density N_e is $10^9 \sim 10^{10}$ cm^{-3} and the plasma diameter is about 4 cm. The value of N_e is axially almost constant.

2. 3. Experimental Procedure and Results

2. 3. 1. Pump frequency nearly equal to the maximum plasma frequency

In Fig. 2. 2 is shown the electron density distribution in the perpendicular position without high frequency input. When the high frequency pump power, whose frequency ω_0 is nearly equal to the maximum plasma frequency ω_{pem}, increases over a certain value, the measured $1/Q$ value changes, as is shown in Fig. 2. 3, having two distinct breaking points. Then the effective collision frequency ν_{eff} ($\ll\omega_0$) can be calculated from the following well known formula[6, 129)]

$$\frac{\nu_{eff}}{\omega_0}=\frac{1/Q-1/Q_0}{2\Delta\omega/\omega_0} \tag{2.1}$$

where Q and Q_0 are the quality values with and without plasma, and $\Delta\omega$ is the frequency shift of the cavity resonance due to the plasma. Equation (2. 1) does not include the plasma volume which is not exactly known, since its effect on Q and $\Delta\omega$ is cancelled.

In Fig. 2. 4 are shown the frequency spectra of the signal picked up by p 3 located on the axis of the plasma. Figure 2. 4 (a) is a typical example of frequency spectra in the range (a) in Fig. 2. 3. Only a sharp spectrum is observed at the frequency ω_0 (f=769 MHz) in the upper figure. In the lower figure of the low frequency range appears a broad noise which is independent on the input power. The value of Q and therefore ν_{eff} are constant in this range. The measured Q_0 is

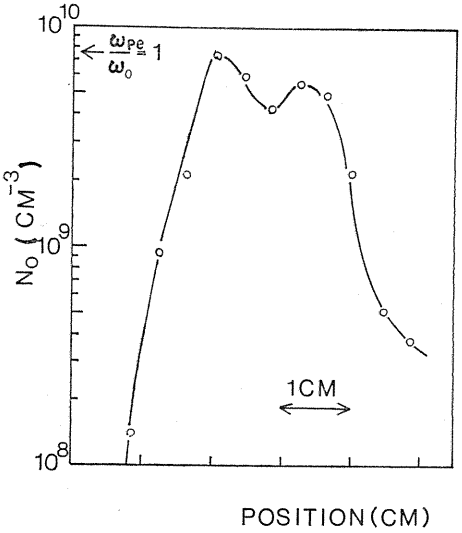

Fig. 2. 2. Electron density distribution measured by P1 in perpendicular position without the high frequency input. The arrow shows the density for $\omega_{pe}/\omega_0=1$. The plasma is produced in Ar, and $p=2\times10^{-4}$ Torr.

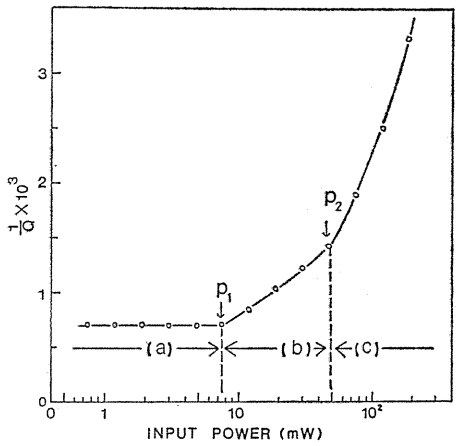

Fig. 2. 3. Measured $1/Q\times10^3$ as a function of the input power into the cavity.

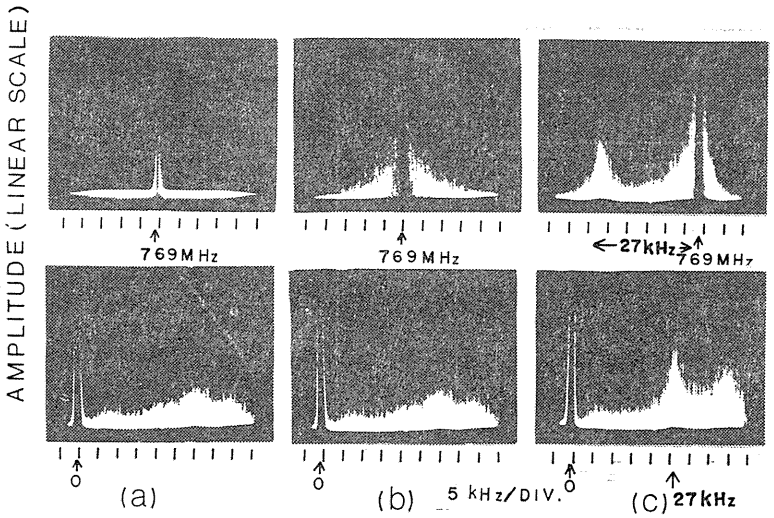

Fig. 2. 4. Upper figures show the high frequency spectra, and lower figures the low frequency spectra. (a) Pump power=5 mW, (b) 30 mW, (c) 200 mW.

about 1400. The value of ν_{eff} estimated from measured $1/Q$ and eq. (2. 1) is quite reasonable considering the electron-neutral collision frequency. Figure 2. 4 (b) corresponds to a medium power of high frequency. At this range (b) of Fig. 2. 3 the spectra of the picked up signal near ω_0 become broader than those of Fig. 2. 4 (a), without any change in the low frequency range. The measured $1/Q$ increases with input power, as is shown in the middle part in Fig. 2. 3. Figure 2. 4 (c) corresponds to a larger power of high frequency. A spectrum of the low frequency ω_2 (f=27 KHz), which must be the ion acoustic wave, is observed as well as a high frequency spectrum of ω_1 (f=769 MHz−27 KHz), which must be an electron plasma wave. It is confirmed that the observed frequencies, ω_1 and ω_2, satisfy the matching condition $\omega_2=\omega_0-\omega_1$. In order to prove the process being a parametric one more clearly, we next examine the dispersion relation of the waves which corresponds to ω_2.

The wave number k_2 is determined by observing the propagating wave patterns of the signal picked up by p 3. In the usual interferometric technique for observing wave propagation, the launched signal can be directly used as a reference signal of the lock-in amplifier. In the present experiment, however, the wave of ω_2 is indirectly excited by the high frequency field of ω_0. Thus, the second fixed P 3 is used to pick up the reference signal. It passes through a narrow band-pass filter in order to select out a particular frequency ω_2. A typical wave pattern is shown in Fig. 2. 5. In Fig. 2. 6, the dispersion relation for the low frequency wave is

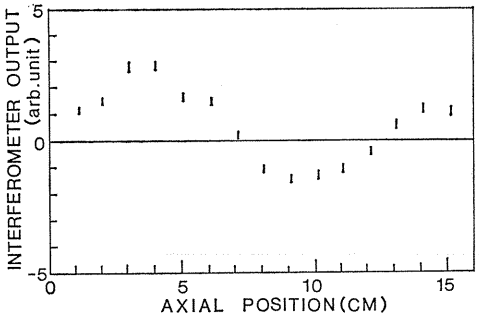

Fig. 2. 5. Interferometer trace of the low frequency wave ω_2 as a function of the axial position.

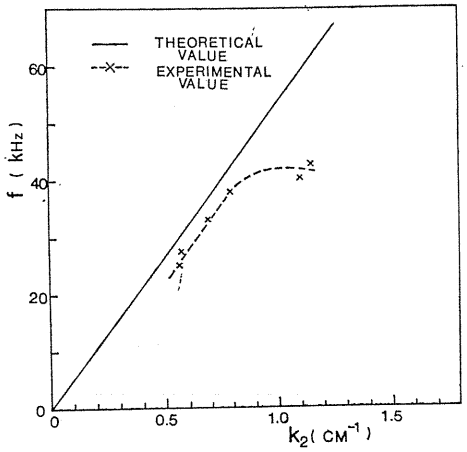

Fig. 2. 6. Dispersion relation of the ion acoustic wave.

plotted as a function of the wave number k_2 with a theoretical line for the ion acoustic wave. The line is calculated from the measured T_e.

The changes in N, T_e and the wave amplitude of the low frequency ω_2 by P 1 at the perpendicular position off the maximum density are shown in Fig. 2. 7 as a function of the input power. The threshold power for the change on N and T_e coincides with each other, whereas that of the wave amplitude is higher than the

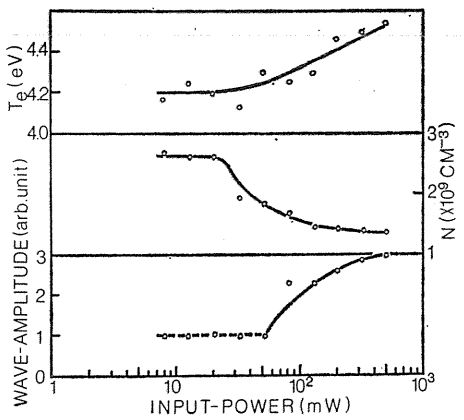

former one. Referring to Fig. 2. 3, we see that the point P_1 is lower than the threshold power for the change of N and T_e, and that the point P_2 is higher than the threshold for N and T_e, The point P_2 coincides with the threshold for the excitation of the low frequency wave.

Fig. 2. 7. T_e, N and wave-amplitude of ω_2 as a function of pump power. Dotted line shows the noise level.

2. 3. 2 Pump frequency higher than the maximum plasma frequency

The density profile shown in Fig. 2. 8 has the point of $\omega_0=\omega_{pe}$ at the periphery of the plasma column. The value of ω_{pe} is determined from the local density which is measured by the Langmuir probe. The relative changes in the density and the electron temperature, i. e., $\Delta N/N_0$ ($\Delta N=N-N_0$) and $\Delta T_e/T_{e0}$ ($\Delta T_e=T_e-T_{e0}$) respectively are shown in Fig. 2. 9, when a constant power of frequency is fed.

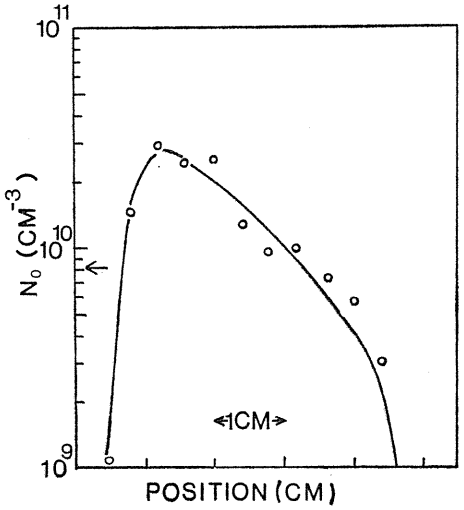

Fig. 2. 8. Electron density distribution in perpendicular position without the high frequency input. The arrow shows the density for $\omega_{pe}/\omega_0=1$.

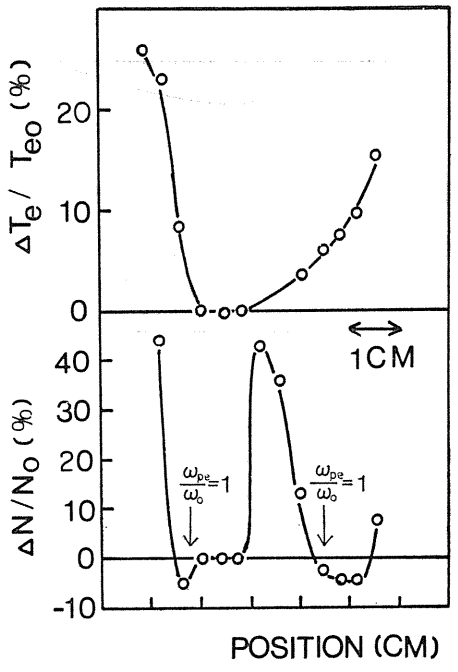

Fig. 2. 9. $\Delta T_e/T_{eo}$ and $\Delta N/N_0$ in perpendicular position.

Here N_0 and T_{e0} mean the values without the high frequency. Around the position of $\omega_0=\omega_{pe}$, $\Delta N/N_0$ is negative, whereas $\Delta T_e/T_{e0}$ is positive. The changes in N and T_e at the position of $\omega_{pe}/\omega_0=1$ in Fig. 2. 9 are shown in Fig. 2. 10 as a function of ω_{pe}/ω_0, when the density is changed by the magnetron power. The absolute value of ω_{pe}/ω_0 is not perfectly correct, since the Langmuir probe characteristic is not yet clearly understood in the magnetic field. Similarly to Fig. 2. 9, $\Delta N/N_0$ decreases and $\Delta T_e/T_{e0}$ increases around the point $\omega_0=\omega_{pe}$. This increase of $\Delta N/N_0$ and $\Delta T_e/T_{e0}$ for low ω_{pe}/ω_0 will be caused by the electrons which move radially owing to the ponderomotive force. In stead of measuring the electric field E inside the cavity which is perpendicular to the density gradient, the electric field outside the cavity is measured using P1. The weak signal which leaks from the cavity is assumed to have the same radial distribution as that inside the cavity. The amplitude of the spectrum at ω_0 displayed on the frequency analyser is plotted in Fig. 2. 11 as a function of radial position. The ordinate is proportional to E. It is clearly shown in Fig. 2. 11 that E is enhanced from the electric field E_i without plasma and has the maximum value at the points A and B where $\Delta N/N_0$ is negative. The dotted line is assumed to be horizontal in such narrow range near the center of the cavity.

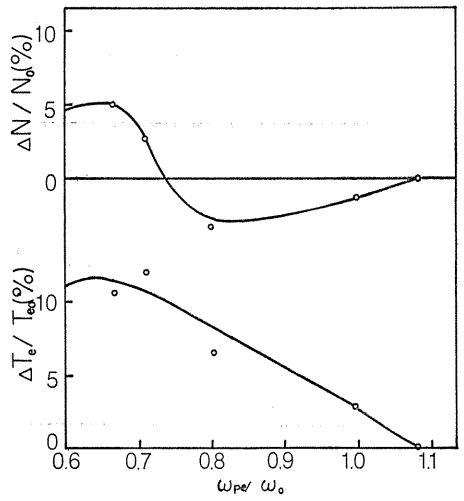

Fig. 2. 10. $\Delta T_e/T_{e0}$ and $\Delta N/N_0$ as a function of ω_{pe}/ω_0 at the position of $\omega_{pe}/\omega_0=1$ in Fig. 2. 9.

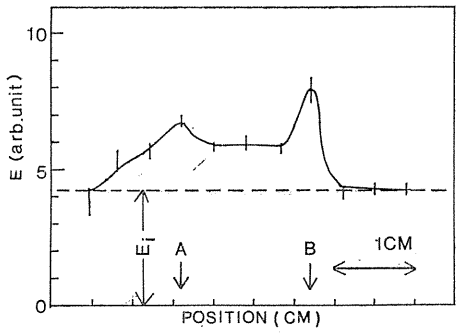

Fig. 2. 11. Radial distribution of the electric field E outside the cavity. Dotted line corresponds the pump electric field intensity. Arrows are the positions where $\Delta N/N_0$ is negative.

2. 4. Theoretical Consideration and Discussions

The first breaking point in Fig. 2. 3 agrees with the threshold value of the field intensity calculated from the theory[11] of the parametric decay of high frequency electric field into the Langmuir and ion acoustic waves in uniform plasmas. However, neither low nor high frequency oscillation, corresponding respectively to ω_2 and ω_1, is detected around this point, as is shown in Fig. 2. 4 (b). When the field intensity is greater than that for the second breaking point, the low and high frequency oscillations are observed, as are shown in Fig. 2. 4 (c).

The theory of the decay process in nonuniform plasma is given by Perkins and Flick.[21] They consider that the unstable region has a finite extent, and the additional loss due to the nonuniformity is the energy loss in the form of the electron plasma waves propagating out of the unstable region. The threshold for the decay process in the nonuniform plasma is defined as the value of the driving electric field, at which the amplitude of the plasma waves in the unstable region is a few times larger than amplitude of the outgoing plasma waves. The second breaking point P 2, which is the threshold for the observable decay waves, is considered to correspond to the threshold of the decay process in the nonuniform plasma, even though no quantitative comparison is made for the threshold values between the theory and our experiment.

The dispersion relation of low frequency waves agrees well with the theoretical one. However, for $k_2 > 0.8$ (cm^{-1}), the experimental value of ω_2 deviates from the theoretical line, and tends to saturate at a level. This discrepancy, which was observed in a current-carrying plasma by Mase and Tsukishima[130] too, might be due to the influence of drift velocity of ions and the nonuniformity of the electron temperature.

For $\omega_0 < \omega_{pem}$, a theoretical model was obtained by White et al.[120] for an injected electromagnetic wave whose polarization is perpendicular to the gentle density gradient of the plasma. Then the electric field in the plasma has a type of Airy function. And the amplification factor of the electric field is derived. Their formulation is not valid under the present condition $k_0 x_0 < 1$, where k_0 and x_0 are respectively the wave number for ω_0 and the scale length of the density gradient. The density N should decrease by the ponderomotive force due to the amplified electric field E. This relationship is written, in our notation, as[84]

$$N = N_0 \exp\left[-\frac{\frac{\omega_{pe}^2}{\omega_0^2} \cdot \frac{\varepsilon_0}{2} \langle E^2 \rangle}{NKT_e} \right] \tag{2.2}$$

Then $\Delta N/N_0 = (N - N_0)/N_0$ can be drawn by the solid line in Fig. 2. 12. The measured value of $\Delta N/N_0$ is also plotted as a function of the field intensity E. The absolute value of E in V/cm is obtained by referring to E_i estimated from the measured Q and input power. The good agreement is found between experimental values and theoretical line.

Ikezi et al.[75] observed a density depression near the point where $\omega_0 \cong \omega_{pe}$ in a large cavity with a nonuniform plasma, where applied electric field is parallel to the density gradient. They found that the density perturbation $\Delta N/N_0$, in our notation, is linearly proportional to the field intensity of ω_0. The dynamic properties of $\Delta N/N_0$ they observed were attributed to a parame-

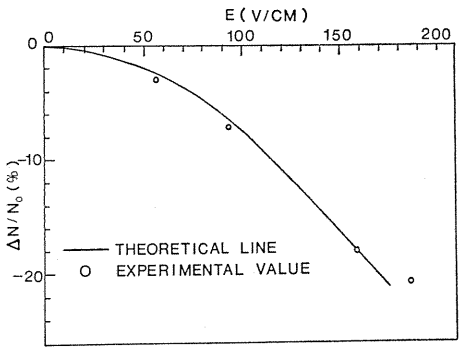

Fig. 2. 12. Relation between $\Delta N/N_0$ and E. Solid line shows the theoretical line calculated from eq. (2.2), and circles the experimental values.

trically excited ion acoustic wave in the presence of the ponderomotive force due to high frequency ω_0. In our case, however, the high frequency field perpendicular to the density gradient is applied steadily on the plasma. Then, the static pressure balance will be achieved between the plasma and the ponderomotive force due to high frequency field.

2. 5. Conclusion

When the intense electric field is applied to the plasma with density gradient, nonlinear interaction appears for both cases $\omega_0 \cong \omega_{pem}$ and $\omega_0 < \omega_{pem}$.

In the first case, the measured collision frequency increases with broadening of the spectrum of signal at ω_0. At the same time, T_e and N change. Afterward ν_{eff} again abruptly increases due to the parametric decay process accompanied with the excitation of the low and high frequency waves. The low frequency wave of ω_2 is identified as an ion acoustic wave from the dispersion relation.

In the second case, where $\omega_0 = \omega_{pe}$ appears in the gradient of the density, T_e increases and N decreases around that position. The decrease of N is explained quantitatively in terms of the ponderomotive force of the amplified electric field.

3. Double Resonance Parametric Process in a Plasma

3. 1. Introduction

Since the theoretical analyses of the parametric excitation of the coupled waves have been published,[7, 8, 11, 19, 21, 31] many experimental results[40, 41, 45, 49, 51, 54, 122, 123, 131] are reported. When the electric field of the one high frequency near the electron plasma frequency is supplied to the plasma, the ion acoustic and the electron plasma waves are parametrically excited over a threshold of the electric field, as predicted by the theory.

Arnush et al. extended the theory to the double resonance parametric process excited by using long wavelength electric fields with two frequencies. This phenomenon is different from the nonlinear mixing of the two electromagnetic waves. They concluded that the total threshold power required for exciting the coupled waves decreased, if the beat between two pump frequencies was chosen equal either to the ion acoustic wave frequency Ω_0, or $2\Omega_0$. The process is efficient for heating the laser produced or magnetically confined plasmas.

In this chapter, the experiment to verify the double resonance parametric excitation is described, where only $2\Omega_0$ is used as the beat frequency. The frequency of Ω_0 is not used, since it is difficult to distinguish experimentally the double resonance parametric process and the nonlinear mixing of the two electromagnetic waves. The present experimental results well agree with the theory.[31]

In 3. 2 is described the experimental apparatus. In 3. 4, the experimental results written in 3. 3 are discussed in comparison with the theory. The results obtained are summarized in 3. 5.

3. 2. Experimental Apparatus

Figure 3. 1 shows the schematic diagram of the apparatus. The plasma is produced by the Lisitano coil[118] fed from the cw magnetron operating at the frequency of 2.45 GHz with the maximum output power of 500 watt.[131] The weak

and homogeneous static magnetic field of about 100 gauss is used to prevent the plasma to radially expand, except the region of the plasma produced by the electron cyclotron resonance. The operating pressure of Argon is 3×10^{-4} Torr. The electron and ion temperatures are 4 eV and 1 eV respectively, and the plasma densitty N is about 10^{10} cm^{-3}.

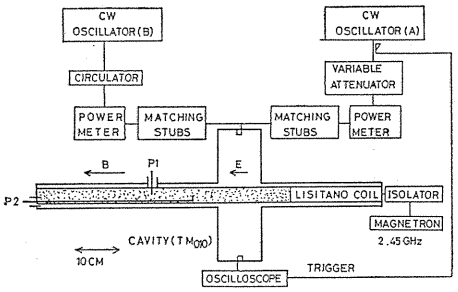

Fig. 3. 1. Schematic diagram.

The outputs from two cw oscillators (A) and (B) with the frequency around 770 MHz are applied to the loop-antenna in the cavity through the variable attenuator or the circulator, the power meters which can measure simultaneously the input and the reflected powers, and the matching stubs. The high frequency electric field inside the cavity of the mode TM_{010} is parallel to the plasma axis and the static magnetic field B. The cavity mode TM_{010} is not almost disturbed by the plasma, since the skin depth of the electric field inside the plasma is much longer than the plasma diameter. The diameter and length of the cavity are respectively 30 cm and 10 cm, and the quality value Q_0 and resonant frequency F_0 are 1400 and 763 MHz in the absence of the plasma.

The oscilloscope triggered by the signal from the oscillator (A) displays the transmitted wave form picked up by another loop-antenna inside the cavity. The electric field inside the cavity is monitored by the wave form displayed on the oscilloscope. To detect the wave signals are used the radially and axially movable Langmuir probes P 1 and P 2, which are inserted into the plasma outside the cavity in order not to disturb the cavity mode. The ion temperature is measured by the multi-gridded probe with the diameter of 5 mm, which is replaced by P 1.

3. 3. Experimental Procedure and Results

In Fig. 3. 2 is shown the dependence of $1/Q$ on the input power P to the cavity for the different resonant frequencies. The upper figure (a) shows the results for two pumps, while the lower one (b) does those for one pump. Then the pump power P in Fig. 3. 2 (a) means the total power from both the oscillators (A) and (B). The output power from the oscillator (B) is constant and less than 1 mW. The frequencies of both the oscillators are selected within the half-width of the resonant curve for the cavity. The resonant angular frequency ω of the cavity increases with the plasma density N.[132] The plasma density which corresponds to the frequency of 790 MHz is two times as large as that for 775 MHz. The value of $1/Q$ for the horizontal line approximately coincides with that calculated by considering the electron-neutral collision frequency. The Q value is calculated here from $Q/Q_0=h\omega/h_0\omega_0$, where h and h_0 are the amplitudes of the transmitted signals read on the oscilloscope at the resonance frequency, and the subscript 0 is the value without the plasma. The quality value Q with the plasma obtained by the present method is more accurate than that determined by the half-width of the resonant curve, because the anomalous absorption by the parametric decay process is sensitive to the intensity of the high frequency electric field. The value of Q_0 is measured by sweeping the frequency of the oscillator.

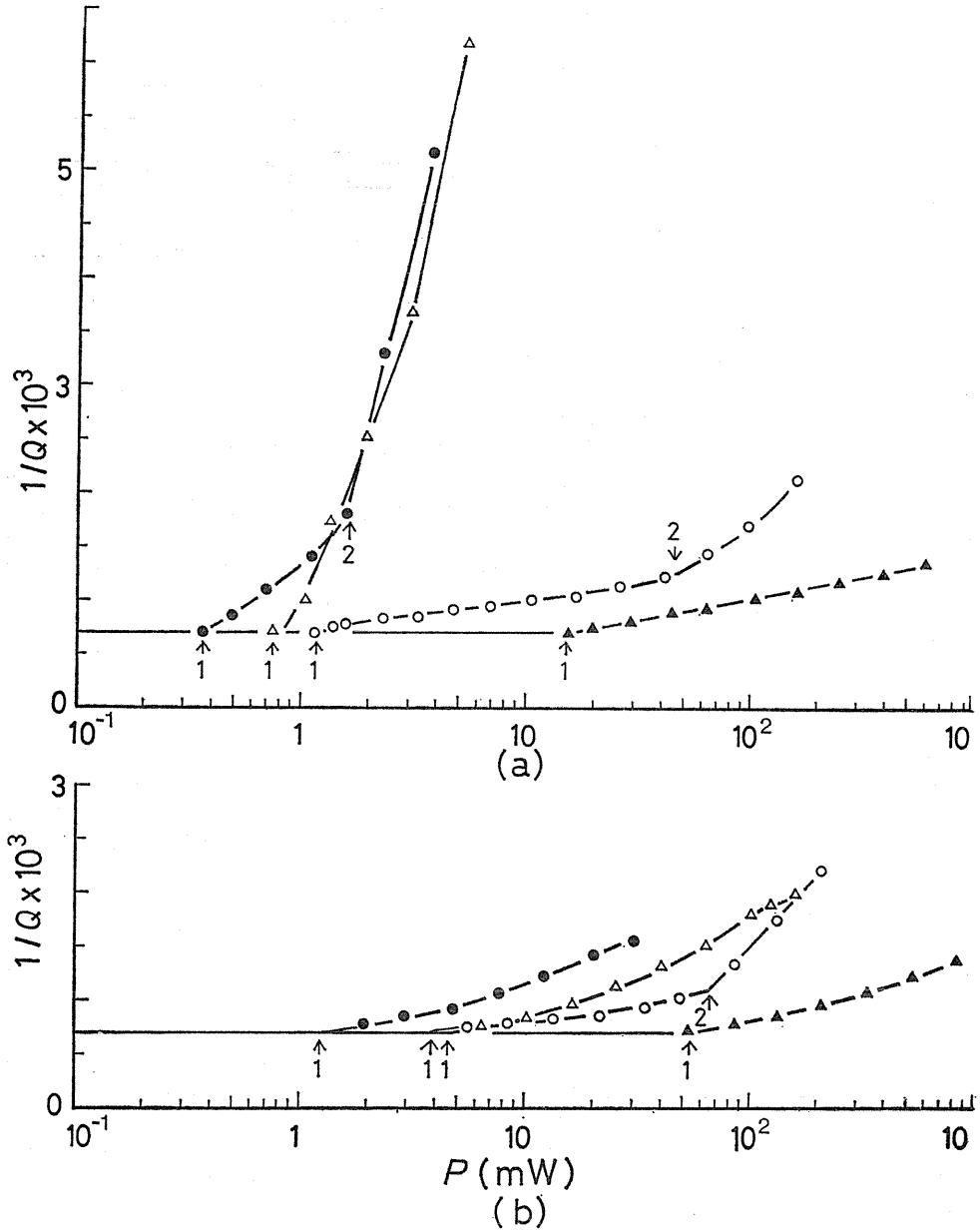

Fig. 3. 2. Measured $1/Q$ as a function of the input power P into the cavity. (a) shows the result for the two pumps, (b) does the results for the single one. 1 means the first breaking point, 2 does the second one. The parameters are the resonant frequency F. Open circles: F=779 MHz, Closed circles: F=781 MHz, Ooen triangles: F=785 MHz, Closed triangles: F=790 MHz.

The frequency difference between two pump waves is chosed twice the ion acoustic wave frequency Ω_0 excited by the one pump wave with the higher frequency of two pump waves. No change of $1/Q$ between the single and two pumps is observed for the frequency difference deviated from Ω_0 and $2\Omega_0$.

The input power P_t at the first and second breaking points, as are shown by 1 and 2 in Fig. 3. 2, is plotted in Fig. 3. 3 as a function of the cavity resonant frequency F. The circles and triangles are respectively P_t at the first and second breaking points. The open and closed signs mean respectively P_t for the two and single pumps. The increase of $1/Q$ means that the electromagnetic wave is absorbed by the plasma. The breaking points are the threshold for the anomalous absorption produced by the parametric instability as discussed later. The threshold for the two pumps is smaller than that for the single pump. The ion acoustic waves cannot be observed for the single pump because of the high damping under the resonant frequency of 775 MHz, therefore Ω_0 cannot be known and the measurement for the two pumps is impossible.

In Fig. 3. 4 are shown the ratios of $\Delta(1/Q)$ to $\Delta(\log P)$ near the first breaking

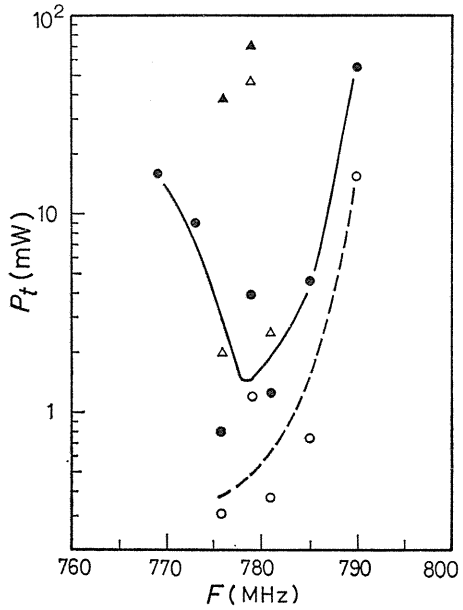

Fig. 3. 3. Threshold power as a function of the resonant frequency. Circles: for the first breaking points, Triangles: for the second ones. Open signs: for the two pumps, Closed: for the single one.

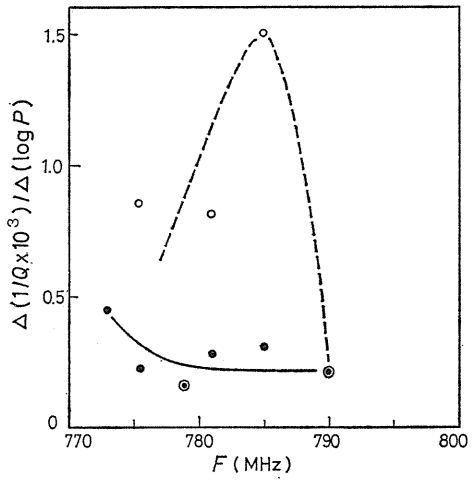

Fig. 3. 4. Gradient of $1/Q\times10^3$ to log P near the first breaking points as a function of the resonant frequency. Open circles: for the two pumps, Closed: for the single one.

points in Fig. 3. 2 as the function of F. The open and closed circles correspond to two and single pumps. The saturation level of amplitude of the waves generally increases with the growth rate, and the saturation level of $1/Q$ increases with the wave amplitude; therefore the saturation level of $1/Q$ increases with the growth

rate. As above assertion means that the ratio of $\Delta(1/Q)$ to $\Delta(\log P)$ increases with the growth rate of the parametric instability, the growth rate for the two pumps is higher than that for the single one as shown in Fig. 3. 4.

In Fig. 3. 5, the amplitude A of the low frequency waves on the spectrum analyzer, which is picked up by the probe P 1, is shown as a function of P. The

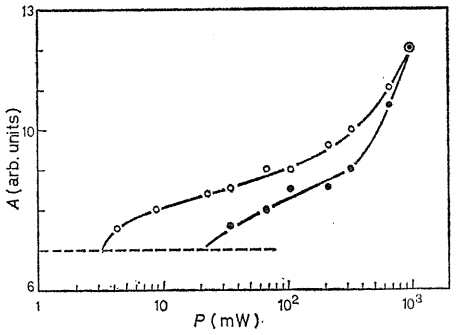

Fig. 3. 5. Amplitude of the low frequency wave as a function of the input power. The broken line is the noise level. Open circles: for the two pumps, Closed: for the single one.

resonant frequency F is 786 MHz. The broken line shows the noise level. The open and closed circles corresdond to two and single pumps respectively. The frequency of the low frequency wave is about 50 kHz. For the single pump, is observed the lower side frequency that satisfies the matching condition of the frequency.[13 1)] The difference between the single and two pumps is larger in the lower power range where the waves are just excited. The difference is smaller in the region of the high input power, since the relative output power from the oscillator (A) to that from the oscillator (B) becomes much larger with the increase of the input power.

3. 4. Theoretical Consideration and Discussions

The experimental results for two pumps are compared with the theory by Arnush et al.[31)] for the double resonance parametric excitation in a plasma. If the beat frequency is chosen approximately equal to the ion acoustic wave frequency or twice, the total threshold power required to excite the ion wave is lower than that for the single pump. Then the linear damping rate ν of the electron wave should be greater than Ω_0. This condition is satisfied in the present experiment. The growth rate just above the threshold is larger than that for the single pump. The minimum values of the thresholds depending on the differences between the pump frequencies and Bohm-Gross frequency are given by

$$\Delta_1\Delta_2=4\nu\Gamma/\omega_{pe}\Omega_0 \tag{3.1}$$

for the two pumps, and

$$\Delta_1^2=(4\sqrt{3}/9)\,(\nu/\Omega_0)\,(4\nu\Gamma/\omega_{pe}\Omega_0) \tag{3.2}$$

for the single one, where Δ_1^2 and Δ_2^2 are the ratios of the electrostatic field energy to the electron thermal one for each pump, Γ the linear damping rate of the ion wave, and ω_{pe} is the electron plasma angular frequency.

The frequency shift of the cavity due to plasma must be considered. If the

plasma fills a part of the cavity, the frequency shift $\Delta\omega$ is expressed by the formula[129, 132]

$$\Delta\omega \cong C\omega_{pe}^2\omega_0/\omega^2 \tag{3.3}$$

where ω_0 is the resonant angular frequency without the plasma, C is the constant dependent on the size of both the cavity and plasma, and the collision frequency is neglected.

The cut-off density N_c is calculated from $\omega=\omega_{pe}$. The radial distributions of the plasma density are shown schematically in Fig. 3. 6 as a parameter F. The error in plasma density calculated from eq. (3.3) is within 13% at $F=792$ MHz compared with the value obtained from the exact solution for $\omega<\omega_{pem}$.[129] The maximum density N_m is smaller than N_c for $F<782$ MHz, N_m is equal to N_c for F of 782 MHz, and N_c exists at the local position of the density slope for $F>$ 782MHz, as are shown in Fig. 3. 6 (a), (b), (c) respectively.

In Fig. 3. 7 is shown the threshold E at the first breaking points in Fig. 3. 3 as a function of N_m. Here N_m is calculated from F using eq. (3.3) and the proper

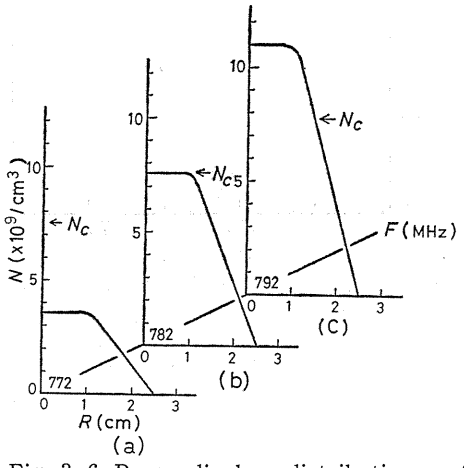

Fig. 3. 6. Perpendicular distributions of the plasma density as a parameter of the resonant frequency. N_c is the cut-off density.

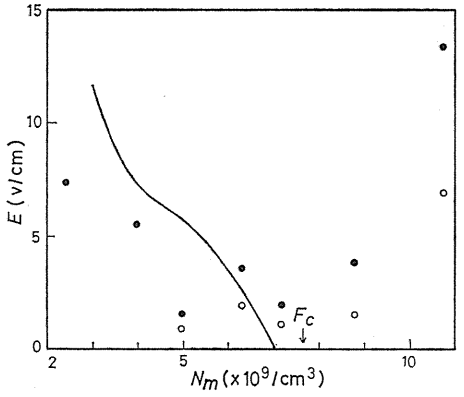

Fig. 3. 7. Threshold of the electric field as a function of the maximum density. The solid line is the theoretical one for the single pump. F_c is the cut-off frequency. Open circles: for the two pumps, Closed: for the single one.

constant C. The experimental value of the electric field E is calculated from $E^2=2PQ/\eta\omega$,[103] where η is a numerical factor depending on the geometry of the cavity, and the net input power P into the cavity is considered as the loss power. The closed and open circles show the threshold for the single and two pumps respectively. The solid line is calculated using $\nu=1.1\times10^6$ and $\Gamma=8.3\times10^2$ from eq. (3.2) for single pump. The increase of the threshold for the lower density is due to the increases in ν and Γ. The theoretical line is approximately close to the closed circles which are the threshold for the single pump. In the region of $N_m>7.6\times10^9$ cm^{-3}, ω is smaller than the electron plasma frequency of the maxi-

mum density ω_{pem} as shown in Fig. 3. 6 (c). The parametric decay instability will appear near the density where the local electron plasma frequency is equal to F. Thus the steep inhomogeneity of the plasma density is essential. The direct comparison between the theory and experiment is not possible because of the difficulty of the measurement of the characteristic length for the density profile inside the cavity.

In Fig. 3. 8 are shown the ratios of the threshold P_{td} for the two pumps to P_{ts} for the single one as a function of F. The horizontal solid line is calculated from eqs. (3. 1) and (3. 2). The experimental values of the open circles agree well with the theoretical one for the double resonance parametric decay process in the neighborhood of the cut-off frequency F_c which is equal to F, since the effect of the inhomogeneity is smaller near N_c in Fig. 3. 6 (b). However, the discrepancy increases with the increase of the resonant frequency. The inhomogeneity of the plasma near N_c as shown in Fig. 3. 6 (c) enhances the effect of the second pump because of the spread for the resonant region.

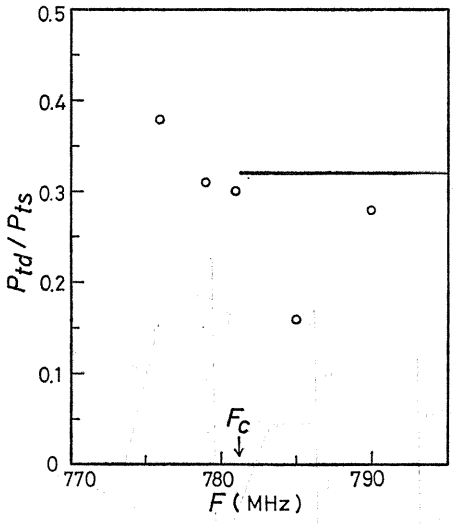

Fig. 3. 8. Ratios of the threshold for two pumps to that for single one as a function of the resonant frequecy. The solid line is the theoretical one for the homogeneous plasma.

The second breaking points are observed near 782 MHz of the cut-off frequency as shown by 2 in Fig. 3. 2. The effect of the inhomogeneous density was described in the previous chapter for the single pump. We consider that the first breaking points show the threshold of the parametric instability for the homogeneous plasma, and the second ones are the threshold, where the growth of the excited wave overcomes the suppression due to the inhomogeneous density. In the region of $F>775$MHz as shown in Fig. 3. 6 (a), the first breaking points are essential because of the uniformity near the maximum density where the parametric process occurs. In the region of $F>782$MHz, where N_c exists on the density slope as shown in Fig. 3. 6 (c), the second breaking points are essential.

The growth rate measured qualitatively agrees with the theory that the growth rate for the two pumps is much larger than that for the single one at just above the threshold.

3. 5. Conclusion

The parametric process is experimentally examined by using the two pumping fields with the beat frequency of twice the ion acoustic frequency. The two pumps have the lower threshold and higher growth rate than the single pump when the linear electron-wave damping rate is greater than the ion acoustic frequency. These phenomena are well explained with the theory[31] of double resonance parametric excitation.

The results presented here suggest that the two pumps are more efficient than the single pump for heating the laser produced and magnetically confined plasmas.

4. Modulational Instability of Electron Plasma Waves Excited by Electric Field in a Resonant Cavity

4. 1. Introduction

The modulational instability of the electron plasma waves has been studied for many years as one of the nonlinear phenomena for heating the plasma by lasers or relativistic electron beams.

The modulational instability for various waves in a plasma has been generally investigated using the nonlinear Schrödinger equation derived from the fluid equations.[62~73] Although the modulational instability of electron plasma waves does not occur in the unmagnetized plasma where the cold ions are assumed,[66] the instability appears in a certain region, if the behavior of warm ions is considered.[79,71] Zakharov reports that the electron plasma waves are unstable in his theoretical analysis, where the equation of ion acoustic wave including the term of ponderomotive force is coupled with the nonlinear Schrödinger equation for the electron plasma wave.[70] Nishikawa et al. used both the nonlinear Schrödinger equation and Korteweg-de Vries equation modified by the ponderomotive force.[71]

The experiments on the modulational instability were reported by some authors.[74~77, 79] Kim et al.[74] observed an enhancement of the high frequency electric field trapped by the density depression in the region where the electron plasma frequency is close to that of the electro-magnetic wave launched from r. f. electrode to the plasma. Wong et al.[77] observed that the electron plasma waves excited by the electron beam collapse into the intense field spikes. Ikezi et al.[79] studied the trapping of the electron plasma wave by the ion acoustic wave. In these reports, there were no direct comparisons between the experiments and the theory derived by Zakharov,[70] since the amplitude of the electron plasma waves observed in these experiments was too large.

In the present chapter the modulational instability of electron plasma wave excited by an electric field in a resonant cavity is described. And a theory is developed to compare with the experimental results extending the basic equations deduced by Zakharov. Then the experimental dependences of the modulational frequency on the amplitude of the electron plasma and modulational waves are in good agreement with the theoretical prediction.

In 4. 2 are described the experimental apparatus and procedure. The experimental results are described in 4. 3, and compared with the theory in 4. 4. The results obtained are summarized in 4. 5.

4. 2. Experimental Apparatus and Procedure

The method of plasma production and the distribution of static magnetic field are the same as those shown in 2. 2. The high frequency field in the cavity of TM_{010} mode is used for exciting the electron plasma waves.

The density of the plasma in the cavity is changed a little when the intensity of the homogeneous magnetic field is varied, since the diffusion loss to the wall

changes at the place where the plasma streams from the region of production to that of the weaker homogeneous field.

The probes P 1 and P 3 as shown in Fig. 2. 1 are electrostatically shielded by the stainless pipes. The high frequency signals superposed on the floating potentials of, and the ion saturation currents to the probe P 1 and P 3 are heterodyne detected, and the output amplitudes are recorded on an X-Y recorder as a function of time.

Ar gas is used with a pressure of 10^{-4} Torr. The electron and ion temperatures measured by Langmuir and multi-gridded probes are about 5 eV and 1 eV respectively. The plasma density and relative density fluctuation are $10^{9}\sim10^{10}\,\mathrm{cm}^{-3}$ and about 1 %.

4. 3. Experimental Results

4. 3. 1. Excitation of electron plasma waves

A high frequency signal of 770 MHz, which corresponds to the resonant frequency of the cavity, is detected by the probe P 3 outside the cavity. In Fig. 4. 1 is shown the amplitude of this signal as a function of the axial distance z from the cavity end. The amplitude has the maximum value at $z=0$, and decreases markedly as the probe is moved outward from the cavity. For $z>1.8$ cm the rate of decrease becomes very small and a fairly uniform distribution is observed. It is found that the fast decreasing part corresponds to the leakage field from the cavity and the fairly constant part stands for an induced electron plasma wave.

The wave number is evaluated from a spatial interferogram of the wave along the axial direction. The spatial interferogram is obtained on the sampling-oscilloscope, to which the probe signal feeds with time axis triggered by a part of the output of the oscillator driving the cavity. The measured values satisfy the dispersion relation of the electron plasma wave considering the inhomogeneity of the plasma density, where the intensity of the static magnetic field is negligibly small. The ratio of the electric field intensity E_0 in the cavity to the intensity E of the

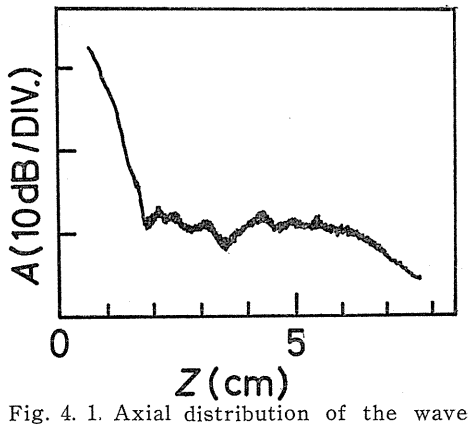

Fig. 4. 1. Axial distribution of the wave amplitude corresponding to the high frequency electric field inside the cavity. The distance z is one outward from the cavity end which is nearer to the probe P 1.

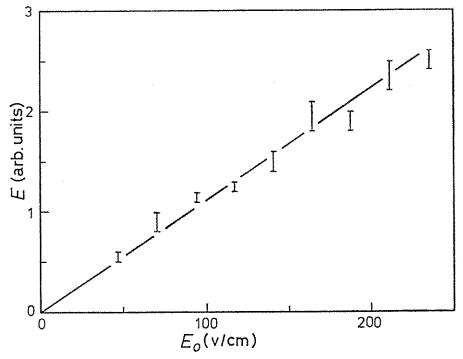

Fig. 4. 2. Dependence of the electric field intensity of electron plasma wave on that inside the cavity at $z=3$ cm.

excited waves is found to be about 25.

In Fig. 4. 2 is shown the dependence of E_0 on E at $z=3$ cm. The E_0 is calculated by the following formula,[103]

$$E_0^2=2PQ/\eta\omega \tag{4.1}$$

where, Q and ω are respectively the quality value and resonant frequency of the cavity, P is the input power to the cavity, and η is a constant value depending on the geometrical size and resonant mode. Since E_0 is directly proportional to E, the electron plasma wave with $E=4$ V/cm is excited by the electric field with $E_0=100$V/cm.

The excitation of the electron plasma wave is due to the mechanism that the velocity modulated electrons by the high frequency field in the cavity are converted to density modulated ones. This mechanism is very similar to that for the wave excitation by the shielded grid.

4. 3. 2 Observation of side band waves

In Fig. 4. 3 are shown the frequency spectra of the floating potential sensed by P3, where center frequency is about 770 MHz. The electron plasma frequency ω_{pem} corresponding to the maximum plasma density in the radial profile can be adjusted by the axially homogeneous magnetic field. The typical photographs of

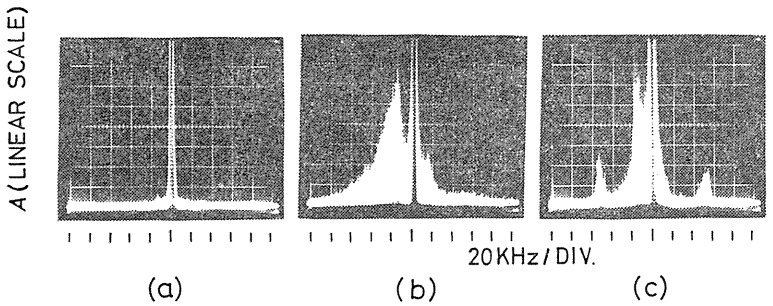

Fig. 4. 3. Frequency spectra near the frequency of 770 MHz at $z=1$cm. (a): $I=65$A, (b): $I=55$A, and (c): $I=45$A.

the frequency spectra produced by the electric field with a little different ω from ω_{pem} are shown in Fig. 4. 3 (a)~(c), where I is the coil current for providing the homogeneous magnetic field. The electro-magnetic wave leaking out the cavity has so large amplitude in Fig. 4. 3 (a) that the amplitude of the excited electron plasma wave with the same frequency is masked. In Fig. 4. 3 (b) is observed the lower side band wave with the larger amplitude than that of the upper side band wave. Moreover, a low frequency wave with a frequency equal to the difference between the lower side band wave and the applied electro-magnetic wave is also observed, although it is not shown in the figure. This means the parametric decay of high frequency electric field into the electron plasma and ion acoustic waves.[131, 133] In Fig. 4. 3 (c) are observed another upper and lower side band waves with the same amplitude and the same frequency difference from the center frequency.

In Fig. 4. 4 is shown the dependence of the amplitude A_1 of lower side band

wave in Fig. 4. 3 on the coil current I, where E_0 is held constant by monitoring the signal from the loop antenna inside the cavity. The closed and open circles show respectively A_1 when both the side band waves with the same amplitude are observed and when the lower side band wave with the larger amplitude than that of the upper side band wave is observed. The regions of (a), (b) and (c) in Fig. 4. 4 correspond to those in Fig. 4. 3. The following experiments are carried out in the region of I, where the amplitude of the closed circles is larger than that of the open circles.

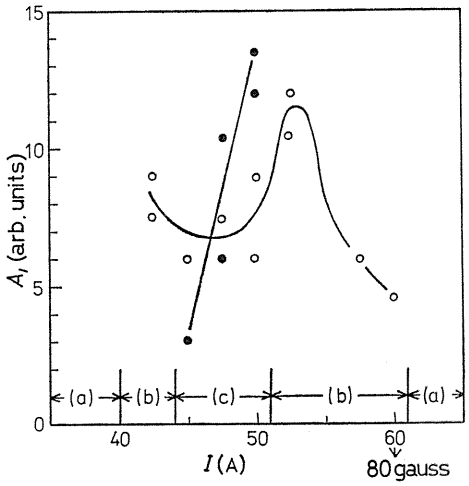

Fig. 4. 4. Dependence of the amplitude A_1 of side band wave on the current I of static magnetic field coil. The closed circles stand for the symmetric side band waves, and open circles do for the asymmetric side band waves.

4. 3. 3. Modulational instability at the small amplitude

In Fig. 4. 5 is shown the temporal waveform of the envelope of the electron plasma wave at $z=5$ cm, where the floating potential of probe P 3 is heterodyne detected. The amplitude of the electron plasma wave is clearly modulated as shown in Fig. 4. 3 (c) and Fig. 4. 5. The frequency and amplitude of the modulational waves increase with E. The both side band waves are not excited by mixing the low frequency waves and electron plasma waves, because the low frequency waves do not observed at the small amplitude.

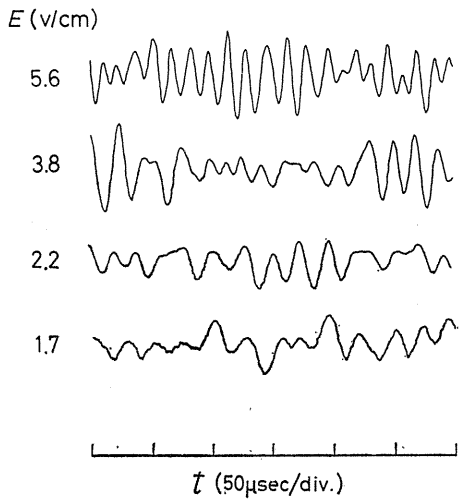

Fig. 4. 5. Detected wave form of electron plasma wave for different E.

The modulational instabilities are studied here in two stages. In the first stage where the amplitude of the electron plasma wave is relatively small, the amplitude modulation occurs and both the higher and lower side band waves are observed. In the second stage where the amplitude is larger than that in the first stage, the low frequency wave is excited in addition to the both side band waves. The boundary between two stages is experimen-

atlly found to be $E=5.5$V/cm which corresponds to $\varepsilon_0 E^2/2NK_bT_e \equiv 5\times10^{-4}$, where N, K_b, ε_0 and T_e are respectively the plasma density, Boltzmann constant, dielectric constant in vacuum and the electron temperature.

Figures 4. 6. and 4. 7. show the dependence of A_1 and F on E. The value of A_1 is proportional to the square of E, and F is directly proportional to E. The error bars in Fig. 4. 7. mean the broad band width of the side band wave. In Fig.

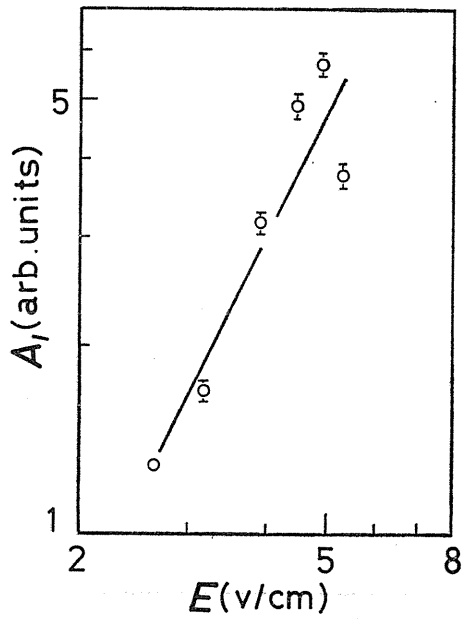

Fig. 4. 6. Dependence of the amplitude of side band waves on the electric field intensity of electron plasma wave.

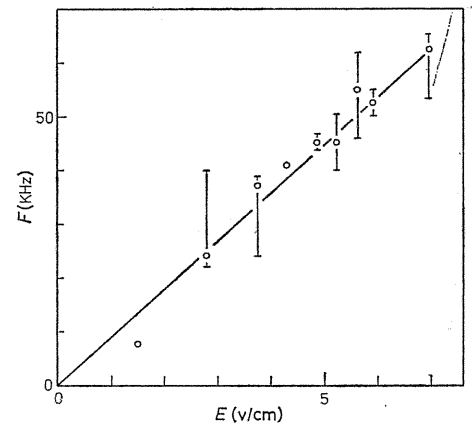

Fig. 4. 7. Dependence of F on the electric field intensity E of electron plasma wave.

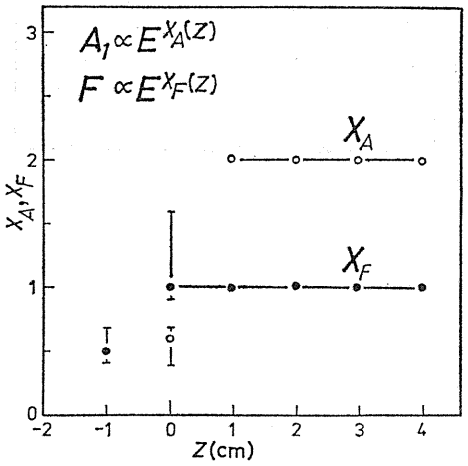

Fig. 4. 8. Axial distributions of X_A and X_F.

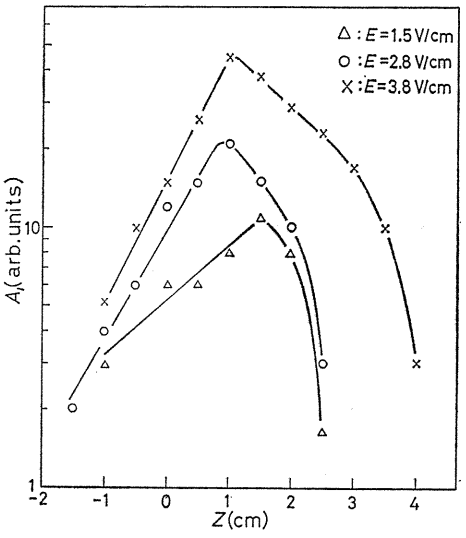

Fig. 4. 9. Axial distributions of the amplitude of side band waves.

4. 8 is summarized the dependence of A_1 and F on E, where X_A and X_F are the indexes of E for A_1 and F respectively. The position of cavity end is shown by $z=0$, and so the negative values of z are the positions inside the cavity. The values of A_1 and F for $5\,\text{cm}>z>0$ are directly proportional to E^2 and E respectively, and it is hard to determine such dependence for $z>5$ cm, since both the side band waves heavily damp out. For $z<0$, the exact measurement is difficult because the cavity mode is disturbed by the probe.

Figure 4. 9 shows the dependence of A_1 on the axial positions for various values of E. The amplitude grows, and then damps exponentially, and the values of z for the maximum amplitude decrease with increasing E for $E<2.8$V/cm. Thus the spatial growth rate of the side band wave increases with the electric field E of the electron plasma waves.

4. 3. 4. Modulational instability at the large amplitude

Figure 4. 10 shows the temporal waveforms of the squared detected electric field $|E|^2$ and the ion saturation current I_{si} at $z=3$cm. The ion density is modulated by the self-modulated $|E|^2$ due to the large amplitude. Then the minimum amplitude of $|E|^2$ coincides with the maximum one of I_{si}. This phenomenon is observed only for $E>5.5$V/cm.

Figure 4. 11. shows the dependence of the amplitude A_2 of low frequency wave and A_1 on z. After A_1 and A_2 grow spatially with about the same growth rate, A_2 propagates with a less damping in spite of the heavy damping of A_1.

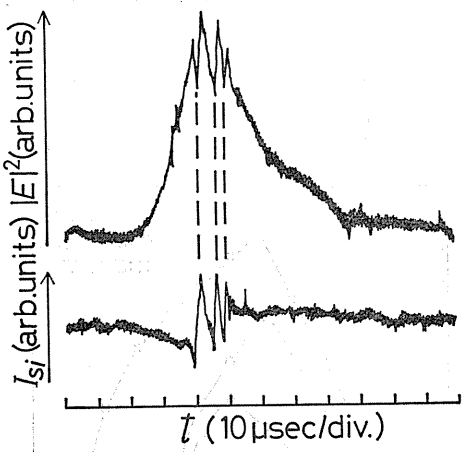

Fig. 4. 10. Waveform of $|E|^2$ and the ion saturation current I_{si} at $z=3$ cm.

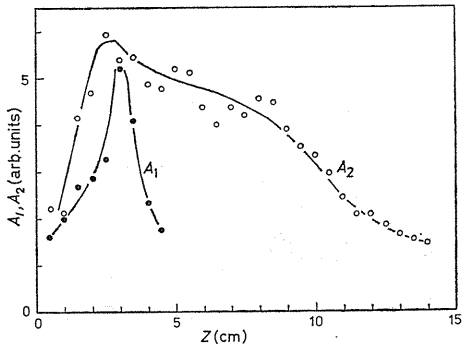

Fig. 4. 11. Axial distribution of the amplitudes A_1 and A_2 of the side band and the low frequency waves.

4. 4. Theoretical Consideration and Discussions

4. 4. 1. Theory of modulational instability

Zakharov[70] derived the equation of ion-acoustic wave including the term of ponderomotive force and the nonlinear Schrödinger equation. The nonlinear Schrödinger equation expresses the electron plasma wave averaged during the "fast time"

of $1/\omega_{pe}$ in the long wave length region. Here, we derive the equations which are convenient to compare with the present experimental results from two equations derived by Zakharov.

The two basic equations[70] are written as

$$i\left(\frac{\partial\psi}{\partial t}+v\frac{\partial\psi}{\partial z}\right)+\frac{3}{2}\omega_{pe}\lambda_D^2\frac{\partial^2\psi}{\partial z^2}-\frac{\omega_{pe}}{2N}\delta N\psi=0, \tag{4.2}$$

$$\frac{\partial^2\delta N}{\partial t^2}-C_s^2\frac{\partial^2\delta N}{\partial z^2}=\frac{\varepsilon_0}{4M}\cdot\frac{\partial^2}{\partial z^2}|\psi|^2, \tag{4.3}$$

where, ψ, ω_{pe}, λ_D, C_s, v and M are respectively the electric field intensity of the electron plasma weves (complex number), the electron plasma frequency, Debye length, ion-acoustic velocity, group velocity of modulational wave and ion mass.

The quantities t, z, δN, v and ψ are normalized by $1/\omega_{pi}$, $1/k_D$, N, C_s and $Nq/k_D\varepsilon_0$, and written as τ, ξ, δN, v and ψ respectively, where ω_{pi}, k_D and q are the ion plasma frequency, Debye wave number and charge respectively. In terms of the normalized quantities, the eqs. (4. 2) and (4. 3) are rewritten as

$$i\left(\frac{\partial\psi}{\partial\tau}+v\frac{\partial\psi}{\partial\xi}\right)+\frac{3}{2}\sqrt{\frac{M}{m}}\frac{\partial^2\psi}{\partial\xi^2}-\frac{1}{2}\sqrt{\frac{M}{m}}\delta N\psi=0, \tag{4.4}$$

$$\frac{\partial^2}{\partial\tau^2}\delta N-\frac{\partial^2}{\partial\xi^2}\delta N=\frac{1}{4}\frac{\partial^2}{\partial\xi^2}|\psi|^2, \tag{4.5}$$

where m is the electron mass. The oscillating quantities are assumed to behave sinusoidally as exp $i(\Omega\tau-K\xi)$. Then we insert δN obtained from eq. (4. 5) into eq. (4. 4), and have the following relation,

$$i\left(\frac{\partial\psi}{\partial\tau}+v\frac{\partial\psi}{\partial\xi}\right)+\frac{3}{2}\sqrt{\frac{M}{m}}\frac{\partial^2\psi}{\partial\xi^2}-\frac{1}{8}\sqrt{\frac{M}{m}}\frac{|\psi|^2}{v^2-1}\psi=0. \tag{4.6}$$

The equation (4. 6) is divided into the real and imaginary parts by putting $\psi=e$ exp $i\phi$, and then the following relations are obtained,

$$\frac{\partial\phi}{\partial\tau}+v\frac{\partial\phi}{\partial\xi}-\frac{3}{2}\sqrt{\frac{M}{m}}\left\{\frac{1}{e}\frac{\partial^2 e}{\partial\xi^2}-\left(\frac{\partial\phi}{\partial\xi}\right)^2\right\}+\frac{1}{8}\sqrt{\frac{M}{m}}\frac{e^2}{v^2-1}=0, \tag{4.7}$$

$$\frac{\partial e}{\partial\tau}+v\frac{\partial e}{\partial\xi}+\frac{3}{2}\sqrt{\frac{M}{m}}\left(2\frac{\partial e}{\partial\xi}\cdot\frac{\partial\phi}{\partial\xi}+e\frac{\partial^2\phi}{\partial\xi^2}\right)=0. \tag{4.8}$$

Next we substitute $E+\delta e$ exp $i(\Omega\tau-K\xi)$ and $\delta\phi$ exp $i(\Omega\tau-K\xi)$ for e and ϕ in eqs. (4. 7) and (4. 8). Then after linearizing we have

$$\begin{pmatrix} -i\Omega+iKv, & -\frac{3}{2}\sqrt{\frac{M}{m}}\frac{K^2}{E}-\frac{1}{4}\sqrt{\frac{M}{m}}\frac{E}{v^2-1} \\ -\frac{3}{2}\sqrt{\frac{M}{m}}EK^2, & i\Omega-iKv \end{pmatrix}\begin{pmatrix}\delta\phi\\ \delta e\end{pmatrix}=0. \tag{4.9}$$

For simplicity of notation, we write $A=1/4\sqrt{M/m}E^2/v^2-1$ and $B=3/2\sqrt{M/m}E$.

From the condition that both $\delta\phi$ and δe are non zero, the following dispersion ralation is derived,

$$\Omega = vK \pm \sqrt{\frac{B^2K^4}{E^2} + \frac{ABK^2}{E}}. \tag{4.10}$$

The unstable region for the amplitude modulation exists for $B^2K^4/E^2 + ABK^2/E < 0$ which requires that v^2-1 is negative. The equation (4. 10) is written as

$$\Omega = \Omega_R \pm i\Gamma, \tag{4.11}$$

where $\Omega_R \equiv vK$, $\Gamma \equiv \sqrt{-(B^2K^4/E^2 + ABK^2/E)}$, and Γ is the growth rate.

The wave number which gives the maximum growth rate is obtained from the relation $d\Gamma/dK = 0$. Then the wave number is tranformed into the frequency using the relation $\Omega_R \equiv vK$,

$$\Omega_R = \pm v\sqrt{-\frac{E^2}{12(v^2-1)}} \tag{4.12}$$

4. 4. 2. Dependence of amplitude and frequency of modulational wave on electric field

The experimental parameters such as T_e and N are substituted to the equation (4. 10) rewritten in terms of the denormalized quantities for the comparison of the experimental results with theory. The wave number is replaced by Ω_R/v, since the relation between the frequency and electric field of the modulational waves is measured in the experiment. The experimental value of v is nearly equal to the ion acoustic velocity. Now, it is assumed that the saturated amplitude of the modulational wave is directly proportional to the growth rate.

Figure 4. 12 shows the theoretical and experimental values of the frequency spectra of the upper side band wave for the various values of E. The measured values agree fairly well with the theoretical curves except for the high frequency side. Small deviations may be due to the mode coupling among the modulational waves.

The modulational frequency Ω_R with the maximum growth rate is theoretically proportional to E from eq. (4. 12), and the maximum growth rate is proportional to E^2 by substituting $K = \sqrt{-E^2/12(v^2-1)}$ to eq. (4. 11). The dependence of E on A_1 and F, which is shown in Fig. 4. 8, well agrees with the theory.

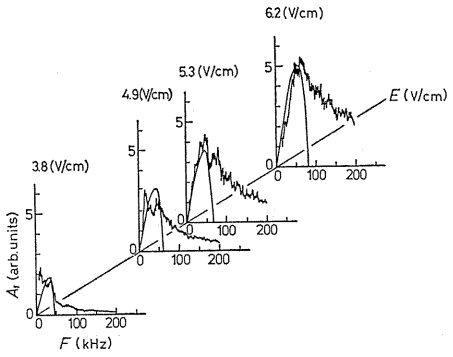

Fig. 4. 12. Frequency spectra of the upper side band waves for different values of E.

4. 4. 3. Modulational and parametric instability

The region of $v^2-1<0$, where the electron plasma wave is unstable for the

modulational instability, corresponds to that of $k<k_D\sqrt{m/M}$, as obtained by substituting the group velocity of the electron plasma wave to the original value v. On the other hand, the parametric instability of decay type occurs for the whole region of the wave numbers.[7, 11, 40, 41, 131, 133] Thus, the instabilities which occur in the region of $k>k_D\sqrt{m/M}$ can be identified as the parametric ones. The wave number can be determined from the frequency by making use of the dispersion relation of the electron plasma wave.

Firstly, let us consider the characteristics of the resonance of the cavity partially filled with the plasma in order to compare the experimental result with theory for the region where two types of unstable waves exist. The relation between the resonant frequency and electron plasma frequency is described by[132]

$$\omega=\omega_0(1+C\cdot\omega_{pe}^2/\omega_0^2), \tag{4.13}$$

where C is a constant depending on the size and mode of the resonant cavity and the diameter of the cylindrical plasma. Figure 4. 13 shows the dependence of the resonant frequency and ω_{pe} on the average density N. If the plasma is radially homogeneous, the modulational and parametric instabilities occur respectively at the density near and under the arrow. The minimum of N exists for the parametric instability, since the threshold values increase with the difference between ω and ω_{pe}.

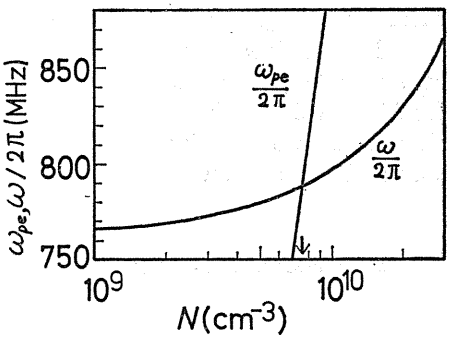

Fig. 4. 13. Dependence of the electron plasma frequency $\omega_{pe}/2\pi$ and the resonant frequency of the cavity $\omega/2\pi$ on the plasma density.

Next, we consider the case where the plasma is assumed to consist of two coaxial cylinders, of which the inner cylinder has a radius of 1 cm and the outer one has a radius of 2 cm. The electron density for $r=2$cm is assumed to be one tenth of the density for $r<$ 1cm. The electron plasma frequency ω_{pem} of the maximum density is equal to ω at about $I=52$A. In Fig. 4. 4, the parametric instability is observed in the region of $62\text{A}>I>40\text{A}$ corresponding to $\omega_{pem}<\omega$, since the region of the plasma density satisfying $\omega_{pe}<\omega$ exists at the radial position of plasma with the density gradient. In the regions of $I>62$A and $I<40$A, the parametric instability is not observed because of the increase of the threshold values due to the sharp density gradient in the radial direction and the large difference between ω and ω_{pe} respectively. The modulational instability is observed at only $\omega\cong\omega_{pem}$ as predicted by the theory.

4. 4. 4. Density fluctuations of ions at the large amplitude

The experimental results of the modulational instability for the electron plasma wave with the large amplitude as shown in Figs. 4. 10 and 4. 11 are interpreted as follows. The fluctuation of ion density with the phase difference of π to the envelope of electron plasma wave is produced by the ponderomotive force of the electron plasma wave.[84, 134] Then the fluctuation of ion density propagates as the

ion acoustic waves after the ponderomotive force becomes insufficient. The side band wave damps more heavily than the ion acoustic wave in Fig. 4. 11, since the electron plasma wave as the carrier wave damps as shown in Fig. 4. 1.

4. 5. Conclusion

The modulational instability excited by the electric field in the resonant cavity is experimentally examined, and compared with the theory. The results obtained are summarized as follows.

(1) The frequency and amplitude of the modulational wave of the electron plasma wave are respectively proportional to the electric field of the electron plasma wave and to the square of it. These phenomena are consistent with the theoretical prediction based on coupling the nonlinear Schrödinger equation describing the electron plasma wave with the equation describing the ion acoustic wave, which include the term of the ponderomotive force.

(2) The modulational instability of the electron plasma waves and the parametric instability of the decay type are experimentally distinguished by control of the plasma density. The region of the density, where two instabilities are observed, agrees with the theory considering the characteristic of the resonant cavity and the radial density gradient.

(3) The low frequency fluctuation of the ion density with a phase difference of π with respect to the envelope of the electron plasma wave is excited for $E>$ 5.5V/cm, and the fluctuation propagates with a moderate damping constant. These phenomena are explained in terms of the ion acoustic wave excited by the ponderomotive force due to the modulated electron plasma wave.

5. Plasma Plugging by High Frequency Field in a Resonant Cavity

5. 1. Introduction

Since the plasma plugging and the heating by the ponderomotive force were proposed in 1956,[87] some theoretical works[84, 85, 93] and computer simulations[92] have been reported. The experiments[96, 99, 103] reported were insufficient to make clear the effect due to the ponderomotive force. For example, Shelby and Hatch[103] produced the plasma by applying the electromagnetic wave with several hundred watts to the cavity of TM_{011} mode, and observed the plasma by the photomultiplier. This work could not confirm the ponderomotive force, because the electromagnetic field was used not only for the plasma plugging but also for production.

Kim et al.[74] and Ikezi et al.[75] observed the amplification of the electric field and a density depression in the neighborhood of the plasma density which corresponds to the cut-off frequency of the electromagnetic wave. They used the pulsed high frequency electric field which directed to the density gradient of the plasma. Authors[131] reported the interactions between the inhomogeneous plasma and the electromagnetic field in steady state for $\omega_{pem}=\omega_0$ and $\omega_{pem}>\omega_0$, where ω_{pem} and ω_0 are the maximum electron plasma frequency and the electromagnetic wave frequency. In the latter case was observed the high frequency electric field amplified with the density decrease and the electron temperature increase.

As an extension of these experiments, the present chapter describes that the plasma can be plugged by the ponderomotive force due to the electromagnetic field

in the cavity under the condition of $\omega_0 \geqq \omega_{pem}$. This work differs from that carried out in the Institute of Plasma Physics, Nagoya University,[98, 101] in points of the applying frequency, the direction of the electric field to the static magnetic field, the feeding apparatus of the electric field and the magnetic field configuration.

In 5. 2, we describe the experimental arrangement. Experimental results given with the method of the measurement in 5. 3 are discussed in comparison with the theory in 5. 4. The results obtained are summarized in 5. 5.

5. 2. Experimental Apparatus

In 2. 2 are shown the method of plasma production and the distribution of static magnetic field with the value of 140 gauss. The high frequency field in the cavity of TM_{010} mode is used for the plasma plugging. The detail about the cavity is written in 2. 2.

The electron plasma frequency is lower than the frequency of the high frequency field in the cavity. The probes P 1 and P 2 as shown in Fig. 2. 1 are used to measure the electron temperature and density in the downstream and upstream sides of the cavity respectively. The axially movable probe P 3 is connected to the spectrum analyzer.

The operating pressure of Ar gas is 10^{-4} Torr. The electron and ion temperatures are about 5 eV and 1 eV respectively. The plasma density and diameter are about $10^9 cm^{-3}$ and 2cm.

5. 3. Experimental procedure and Results

In Figs. 5. 1 and 5. 2 are shown the radial distributions of T_e and N_e measured by P 2 and P 1. Each figure shows the values in the upstream and the downstream sides. The geometrical center of the apparatus is indicated by the radial position $R=0$. The input power P_0 is 1 watt and the resonance frequency of the cavity is 767 MHz. The influence of the electromagentic field to the probe characteristic is negligible, since the outside of the cavity is the cut-off region for the electromagnetic wave. It is confirmed by the fact that the ratio of the electric field at the position of the probe to that in the cavity is less than 10^{-4}. The field is measured by picking up the signal of the high frequency with P 3 connected to the spectrum analyzer. When the electromagnetic wave is fed to the cavity, the density N_e in the upstream side increases up to the maximum value of 180% at $R=1.2$cm for the density without input power, and then the temperature T_e is little changed. In the downstream side, N_e decreases down to the maximum value of 43% at $R=1.2$cm, and T_e increases a little.

In Figs. 5. 3 and 5. 4 are shown $\Delta N_e/N_{e0}$ and $\Delta T_e/T_{e0}$ of the upstream and the downstream sides. These values are measured by changing the input power P_0 through the variable attenuator, where N_{e0} and T_{e0} are $1.2\times10^9 cm^{-3}$ and 3.4 eV respectively for no input power, ΔN_e and ΔT_e are the difference between the values with and without input power. Then P 1 and P 2 are almost situated on the axis of the apparatus. The input power P_0 means the net input power which is the difference between the power fed to the loop-antenna in the cavity and the reflected one. In Fig. 5. 3 is shown the density increase with the input power in the upstream side. For example, the input power of 10 watt produces the density increase of 57% and the small change of T_e. In Fig. 5. 4. are shown the decrease of N_e and increase of T_e with the input power in the downstream side.

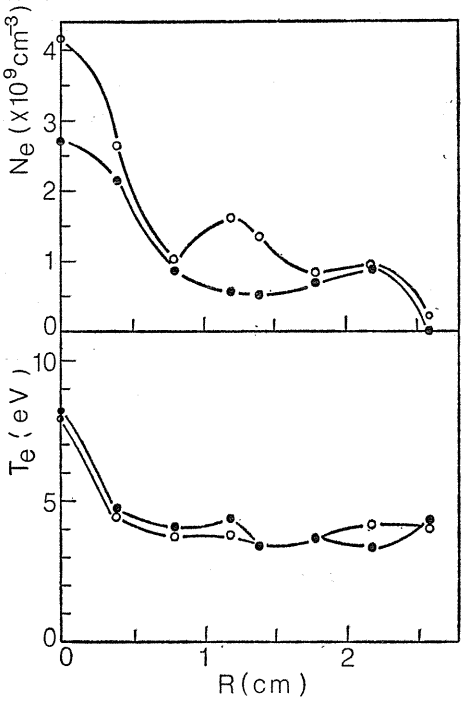

Fig. 5. 1. Radial distributions of the electron temperature and the density in the upstream side. Open circles show the case with electric field, and closed circles without electric field. Cut-off density is 7.3×10^{9} cm^{-3}.

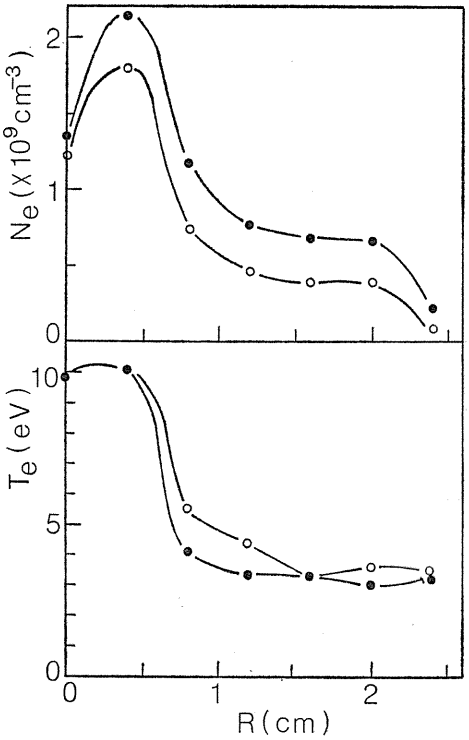

Fig. 5. 2. Radial distributions of the electron temperature and the density in the downstream side. Open circles show the case with electric field, and closed circles without electric field.

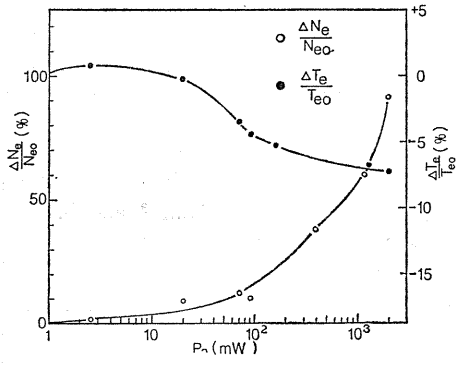

Fig. 5. 3. Dependence of $\Delta N_e/N_{eo}$ and $\Delta T_e/T_{eo}$ on the input power in the upstream side.

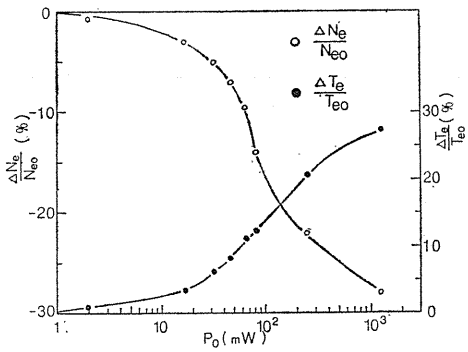

Fig. 5. 4. Dependence of $\Delta N_e/N_{eo}$ and $\Delta T_e/T_{eo}$ on the input power in the downstream side.

In Fig. 5. 5 are shown the frequency spectra of the floating potential picked up by P3 at a position near the cavity, where P_0 is 2.5W. The Figs. 5. 5 (a) and (b) show the frequency spectra of the low and the high frequency ranges, respectively. Upper and lower side frequencies ω_1 are observed at the separated points from the center frequency of 767 MHz. The amplitude of the side waves ω_1 and the corresponding low frequency wave ω_2 increases with P_0. The difference between the center frequency and ω_1 increases with the amplitude. The frequencies of ω_1 and ω_2 are not observed for P_0 less than a certain value.

After the high frequency signal picked up by probe P3 is converted to an intermediate frequency using the local oscillator, the i. f. signal is firstly passed through a filter with a narrow band width and then fed to an i. f. amplifier. Finally the amplitude of the output of the i.f. amplifier is displayed as a function of time on the oscilloscope. Then the amplitude of the high frequency signal is shown in Fig. 5. 6. The amplitude of the high frequency is modulated by ω_2 which

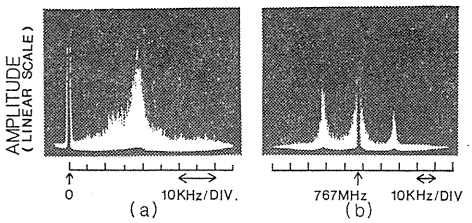

Fig. 5. 5. (a) Low frequency spectrum, (b) High frequency spectrum.

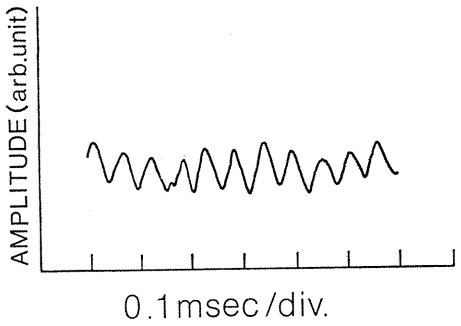

Fig. 5. 6. Wave form of the envelope for the high frequency.

corresponds that in Fig. 5. 5 (a). This amplitude modulation is not observed for P_0 under a certain value. The ion temperature is not changed by P_0 within the resolution of the energy analyzer.

5. 4. Theoretical Consideration and Discussions

The high frequency electric field along the magnetic field is produced by applying the electromagnetic wave to the cavity. Only the small fraction of the electromagnetic wave leaks outside the cavity, since the cut-off condition is satisfied by the geometry of the apparatus. The flowing plasma is pushed back by the ponderomotive force which is produced by the axial inhomogeneity of the high frequency electric field. In other words, we adopt a model that the electric field E_z in the cavity becomes the barrier against the plasma flow.

Ponderomotive force[84, 86] f_s is given by

$$f_s = -\frac{\omega_{ps}^2}{\omega_0^2}\nabla\left\langle\frac{\varepsilon_0}{2}E_z^2\right\rangle, \tag{5.1}$$

considering $E_r = E_\theta = 0$, where s stands for electrons or ions, ω_0 the frequency of the applied electromagnetic wave, ω_{ps} the electron or the ion plasma frequency, and ε_0 represents the vacuum dielectric constant, z is the direction of the static

magnetic field, The bracket means averaging over one period of oscillation.

For investigating the effect of the ponderomotive force to the plasma, the motion and Poisson equations are coupled. The equations of motion are modified by the presence of the ponderomotive force of eq. (5. 1) as an external force, where only the slow motion is considered for the electrons. The basic equations are written as

$$mN_e\left(\frac{\partial v_e}{\partial t}+v_e\frac{\partial}{\partial z}v_e\right)=-N_eeE+f_e-\frac{\partial}{\partial z}(N_eKT_e), \tag{5.2}$$

for electrons

$$MN_i\left(\frac{\partial v_i}{\partial t}+v_i\frac{\partial}{\partial z}v_i\right)=N_ieE+f_i-\frac{\partial}{\partial z}(N_iKT_i), \tag{5.3}$$

for ions. The Poisson equation is

$$\frac{\partial E}{\partial z}=\frac{e(N_i-N_e)}{\varepsilon_0}, \tag{5.4}$$

where m, M, v, e, K and E are the electron mass, ion mass, velocity, charge, Boltzmann constant and electric field produced by the charge separation.

We assume the charge neutrality and equal velocity as

$$N\equiv N_e\cong N_i, \tag{5.5}$$

$$v\equiv v_e=v_i. \tag{5.6}$$

The sum of eqs. (5. 2) and (5. 3) is written as

$$(m+M)N\frac{\partial v}{\partial t}+(m+M)N\frac{\partial}{\partial z}\frac{v^2}{2}=f_e+f_i-\frac{\partial}{\partial z}NK(T_e+T_i), \tag{5.7}$$

where $eE(N_i-N_e)$ of the second order is dropped. The steady state is calculated from eq. (5. 7) as

$$\frac{\partial}{\partial z}\left\{\frac{1}{2}Mv^2+\frac{e^2}{m\varepsilon_0\omega_0^2}\left\langle\frac{\varepsilon_0}{2}E_z^2\right\rangle\right\}+K(T_e+T_i)\log N=0, \tag{5.8}$$

where $m\ll M$ is used. As the flow velocity is slow, the solution of eq. (5. 8) is derived as

$$N=N_0\exp\left\{-\frac{\dfrac{e^2}{2m\omega_0^2}\langle E_z^2\rangle}{K(T_e+T_i)}\right\}, \tag{5.9}$$

where N_0 is the plasma density without the high frequency field.

The changes in the density measured are shown in Fig. 5. 7 as a function of the high frequency electric field. The broken line is drawn through four points deviated from the theoretical line, which is obtained from eq. (5. 9) considering $\Delta N_e=N_e-N_{e0}$. The E_z of eq. (5. 9) is measured from the amplitude of the signal on the oscilloscope connected with the loop-antenna in the cavity. Its absolute value is calculated from $E_z{}^2=2P_0Q/\eta\omega_0$[10 3)], where η is a constant determined by

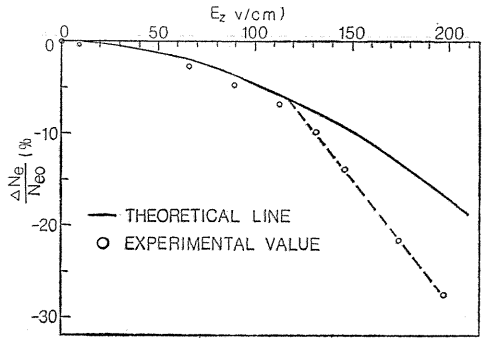

Fig. 5. 7. Dependence of $\Delta N_e/N_{eo}$ on the electric field in the downstream side.

the geometry of apparatus. The experimental values in Fig. 5. 7 agree with the theoretical line under the electric field of 110V/cm, and are linearly proportional to the electric field for the higher field. We think that the point of intersection between the horizontal axis and the broken line shows the threshold value of the transition from the exponential type to the linearly proportional one.

We believe that the modulational instability occurs in the linearly proportional range, since the amplitude of the high frequency is self-modulated by the low frequency, as is shown in Figs. 5. 5 and 5. 6.

Ikezi et al.[75] reported that the relation between the density and the electric field at $\omega_0 \cong \omega_{pe}$ is not dependent on the static pressure balance, when the modulational instability occurs. Nishikawa et al.[71] and Mima et al.[135] explained theoretically their experiment. The broken line in Fig. 5. 7 may correspond to their phenomenon, but our experiment is carried out under the condition of $\omega_0 > \omega_{pem}$. We suppose that the inhomogeneity of the applied high frequency electric field produces the modulational instability in spite of a different condition.

The electron temperature T_e at radial positions does not change as average in the upstream side, as shown in Fig. 5. 3. However, T_e increases in the downstream side, as is shown in Fig. 5. 2. The reason is that the high energy electrons pass through the cavity.

5. 5. Conclusion

In the present experiment are observed the plasma plugging due to the ponderomotive force and the amplitude modulation.

The density N_e increases with a little change of T_e in the upstream side of the cavity. The density N_e decreases with some increase of T_e in the downstream side. The relation between the density decrease and the electric field is in quantitative agreement with the theory which includes the ponderomotive force, when the high frequency electric field is lower than a certain threshold value. The density decrease is linearly proportional to the electric field for the higher value, and at the same time the amplitude of the high frequency signal is modulated by a low frequency.

Since the high intensity of the electric field is easily obtained by the high Q-value of the cavity, the extension of the present technique to the high density and high temperature plasma may be possible by using the microwave of higher power and frequency.

6. Suppression of Plasma Loss from a Mirror End by the Ponderomotive Force of High Frequency Field

6. 1. Introduction

Mirror machines which have been investigated for many years have some disadvantages as fusion reactors.[136, 137] One of those is that the loss from both ends of the mirror machines seriously restricts the confinement time of the plasma.

In order to reduce the end loss, some proposals to use the high frequency or electrostatic fields have been reported by many authors.[87,93,97,100,102,134,138,139] In the experiments[97, 100, 102] of plasma confinement by r. f. field carried out at the frequency near the electron and ion cyclotron resonances, it is difficult to separate the effect of the ponderomotive force and the heating of electrons and ions. On the other hand, Shelby and Hatch[103] report that the plasma can be confined even without cyclotron resonance by the quasi-potential well produced by r. f. field in the cavity. In their work, the ponderomotive force is not quantitatively confirmed since the r. f. field is used for both the plasma production and confinement.

In the present chapter, it is possible to study quantitatively the suppression of plasma loss at a mirror end by applying an r. f. field to the plasma separately produced by another r. f. oscillator. The used frequency is a little higher than the electron plasma frequency. Since the direction of electric field in the cavity operated at TM_{010} mode coincides with the plasma axis, the cyclotron resonance is avoided to achieve the adiabatic confinement. The experimental results agree well with the theoretical analysis based on the ponderomotive force with the mirror magnetic field.

In 6. 2 is given the theoretical analysis. The experimental apparatus and procedures are described in 6. 3, and the experimental results are discussed in comparison with the theory in 6. 4. The obtained results are summarized in 6. 5.

6. 2. Theory

It is theoretically analysed that the plasma loss at a mirror end is suppressed by the ponderomotive force produced by the electric field in the resonant cavity. The axial distribution of the magnetic field is shown in the bottom of Fig. 6. 2, where the intensity B_1 at one end is variable, while B_0 at the another end and B at the mirror center are fixed. Then it is assumed that the plasma, which is produced near B_0 and flows toward the mirror center, has a half Maxwellian velocity distribution.

At first, the density of electrons reflected by the mirror field with B_1 is theoretically deduced as follows. The conservation of energy and the adiabatic invariance of the magnetic moment are expressed by

$$\frac{1}{2}mv_0^2=\frac{1}{2}mv^2, \tag{6.1}$$

$$\frac{mv_{\perp 0}^2}{2B_0}=\frac{mv_\perp^2}{2B}, \tag{6.2}$$

where, the velocity v and B with and without subscript of 0 mean those at the

position of B_0 and in the region of B, and m and the subscript $\perp$ are the electron mass and the perpendicular component to the magnetic field. From eqs. (6. 1) and (6. 2), we obtain

$$\theta = \sin^{-1}(\sqrt{R_0}\sin\theta_0), \tag{6.3}$$

where $R_0 = B/B_0$, $v_\perp = v\sin\theta$ and $v_{\perp 0} = v_0\sin\theta_0$. The velocity distribution of the electrons in the region of uniform magnetic field B changes from the half maxwellian velocity distribution to the following one, considering the decrease of the magnetic field from B_0 to B and eq. (6. 3).

$$f_e = 2\left(\frac{m}{2\pi KT_e}\right)^{\frac{3}{2}} \frac{v^2}{R_0} \frac{\cos\theta\cdot\sin\theta}{\sqrt{1-\frac{1}{R_0}\sin^2\theta}} \exp\left(-\frac{mv^2}{2KT_e}\right), \tag{6.4}$$

where K and T_e are the Boltzmann constant and the electron temperature, and $\theta < \sin^{-1}\sqrt{R_0}$. The density n_r of electrons reflected by the mirror field B_1 is written as

$$n_r = 1 - \int_0^\infty dv \int_0^{2\pi} d\varphi \int_0^{\sin^{-1}\sqrt{\frac{1}{R}}} f_e\, d\theta = \sqrt{1-\frac{1}{R\cdot R_0}}, \tag{6.5}$$

where R is B_1/B, and $B_1 > B_0$. Then the plasma density n_m in the region of uniform magnetic field is

$$n_m = 1 + n_r, \tag{6.6}$$

where the quasi-neutrality is assumed. The values of n_r and n_m are normalized by the plasma density in the region of B at $R=1$.

Next, we consider the effect of r. f. field in the cavity introduced at the position shown in Fig. 6. 2. The quasi-potential ψ produced by the ponderomotive force is written as[88]

$$\psi = \frac{e^2E^2}{4m\omega^2}, \tag{6.7}$$

where ω and E denote the frequency of the applied r. f. field and its intensity. The end stopper effect of the r. f. field converts the loss-cone distribution of electrons into loss-hyperboloid one, when the electrons are reflected by the mirror field.[93] Then it is assumed that the ions are reflected by the ambipolar potential ϕ, which is produced by the charge separation between the ions and electrons. Thus the necessary potential ψ for the plasma confinement should be the sum of the kinetic energy of the ions and electrons.

The loss-hyperboloid angles θ_{ci} are[93]

$$\theta_{ci} = \sin^{-1}\left\{\left(1-\frac{2\phi}{Mv^2}\right)/R\right\}^{\frac{1}{2}} \quad \text{at} \quad v \geq \left(\frac{2\phi}{M}\right)^{\frac{1}{2}}, \tag{6.8}$$

$$\theta_{ci} = 0 \quad \text{at} \quad v \leq \left(\frac{2\phi}{M}\right)^{\frac{1}{2}}, \tag{6.9}$$

for ions, where M is the ion mass, and

$$\theta_{ce}=\sin^{-1}\left[\left\{1-\frac{2(\psi-\phi)}{mv^2}\right\}/R\right]^{\frac{1}{2}} \quad \text{at} \quad v\geq\left\{\frac{2(\psi-\phi)}{m}\right\}^{\frac{1}{2}}, \tag{6.10}$$

$$\theta_{ce}=0 \quad \text{at} \quad v\leq\left\{\frac{2(\psi-\phi)}{m}\right\}^{\frac{1}{2}}, \tag{6.11}$$

for electrons. In this calculation, we should take the ratio of the magnetic field intensity at the position of the cavity to B. The error for using $R=B_1/B$ is negligibly small. The plasma loss n_{il} and n_{el} at the mirror end is

$$n_{il}=\int_0^{2\pi}d\varphi\int_{\sqrt{\frac{2\phi}{M}}}^{\infty}dv\int_0^{\theta_{ci}}f_i d\theta, \tag{6.12}$$

for ion, and

$$n_{el}=\int_0^{2\pi}d\varphi\int_{\sqrt{\frac{2(\psi-\phi)}{m}}}^{\infty}dv\int_0^{\theta_{ce}}f_e d\theta, \tag{6.13}$$

for electrons, where f_i is the same expression as eq. (6. 4) for f_e except that M and the ion temperature T_i are substituted for m and T_e.

The ambipolar potential ϕ can be obtained by assuming the charge neutrality that n_{il} of eq. (6. 12) is equal to n_{el} of eq. (6. 13). Then n_{el} can be calculated from eq. (6. 13) using the value of the potential ϕ obtained. The plasma density n in the region of the uniform magnetic field can be deduced as

$$n=1+(1-n_{el}). \tag{6.14}$$

The suppression ratio $-\Delta n/n_{ml}$ of the end loss by the ponderomotive force is deduced as

$$\frac{-\Delta n}{n_{ml}}=\frac{\int_0^{2\pi}d\varphi\int_0^{\infty}dv\int_0^{\sin^{-1}\sqrt{\frac{1}{R}}}f_e d\theta-n_{el}}{\int_0^{2\pi}d\varphi\int_0^{\infty}dv\int_0^{\sin^{-1}\sqrt{\frac{1}{R}}}f_e d\theta}, \tag{6.15}$$

for $R_0R\geq 1$, where the denominator is the end loss n_{ml} for the mirror field without r. f. field, and the numerator is the difference of n_{el} from n_{ml}.

This theory is schematically explained by Fig. 6. 1, which shows the velocity space in the region of the uniform magnetic field for the distribution of the

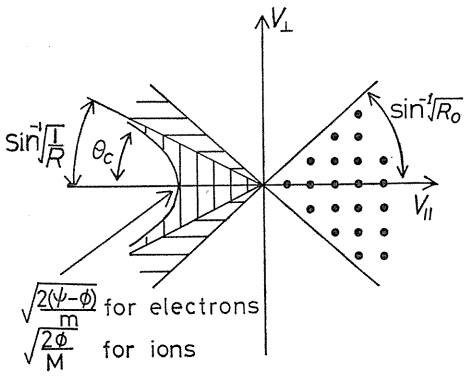

Fig. 6. 1. Schematic velocity distribution of plasma at the mirror center.

magnetic field in Fig. 6. 2. The dotted region contains the charged particles flowing from the region of the plasma production toward the mirror field. The horizontally and vertically hatched regions contain the particles reflected by only the mirror field and by the ponderomotive force with the mirror field respectively.

6. 3. Experimental Apparatus and Procedure

The schematic diagram of the experiment is shown in Fig. 6. 2. The plasma is produced by the Lisitano coil,[118] to which a microwave power is supplied from a cw magnetron operating at the frequency of 2.45GHz. The magnetic field B_0 is 875 gauss, which satisfies the condition of the electron cyclotron resonance. The magnetic field B is 135 gauss, and B_1 is variable.

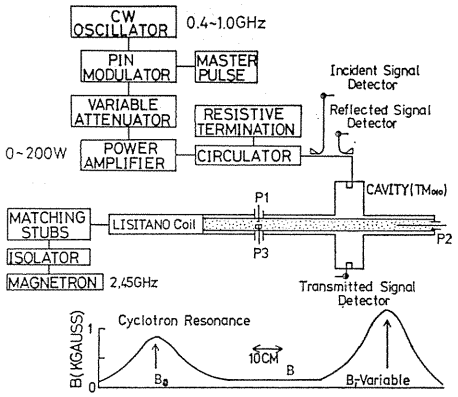

Fig. 6. 2. Schematic diagram of the experiment.

After the output power of a few watts from another cw oscillator is modulated by the master pulse, the power is amplified up to 200 watts. Then the r. f. power is fed to the loop-antenna inside the cavity operated at TM_{010} mode through the circulator and two directional couplers. The cavity has the diameter of 30 cm, the length of 10 cm, the Q-value of 2500 and resonant frequency of 763MHz without the plasma. Another loop-antenna is connected to the oscilloscope through the square-law detector in order to monitor the electric field in the cavity. The r. f. field leaking through two holes of the cavity damps strongly because of the cut-off effect of the geometrical size of the holes.

The ion density and temperature in the region of the uniform magnetic field are measured by the multi-gridded probe P 3 with a diameter of 5 mm. The electron density and temperature are measured by the Langmuir probe P 1 with a diameter of 1 mm. Both probes are radially movable. The Langmuir probe P 2 is used to measure the plasma density and the electron temperature of the plasma at the mirror end. The experimental values of 64 data obtained with the time interval of 0.1 sec are averaged by the data-processor (Iwatsu-1330).

The operating pressure of Ar gas is 10^{-4} Torr, and the ion and electron temperatures are about 0.4 and 4 eV respectively. The plasma density and Larmor radius of ions are $10^{9}\sim10^{10}cm^{-3}$ and 4.3 cm. The radius of apparatus is 2.7 cm. The plasma is thought to be collisionless, since the ion-ion mean free path is comparable to the vessel length.

6. 4. Experimental Results and Discussions

6. 4. 1. Mirror effect without r. f. field

The mirror effect is investigated in the axial distribution of the magnetic field as shown in Fig. 6. 2. In Fig. 6. 3 is shown the radial distribution of electron saturation current I_{se} in the region of the uniform magnetic field as a parameter of mirror ratio R. The electron saturation current I_{se} increases with R. Since

the measured electron temperature does not change with R, I_{se} is thought to correspond to the relative electron density.

In Fig. 6. 4 is shown I_{se} at $r=0$ shown in Fig. 6. 3 as a function of R, where the theoretical curve is calculated from eq. (6. 6). When B_0 is equal to B_1, the

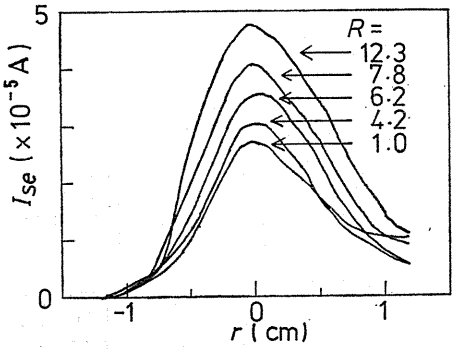

Fig. 6. 3. I_{se} as a function of r for the different values of R at the mirror center.

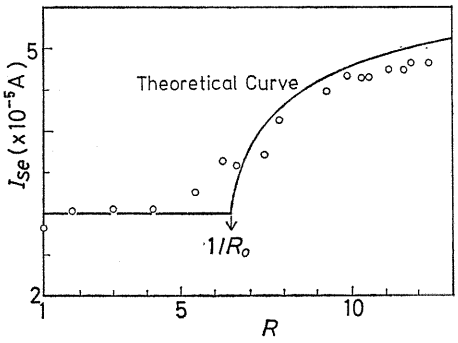

Fig. 6. 4. I_{se} as a function of R at the mirror center.

mirror ratio R is 6. 4. A breaking point appears at $R=6.4$ for the theoretical line. The experimental values almost lie on the theoretical line except near the breaking point. Such deviation near that point may be caused by a fact that the charged particles scattered by the microwave field for the plasma production prevent the plasma having theoretically assumed half maxwellian distribution.

6. 4. 2. R. F. field effect in the mirror field

Figure 6. 5 shows the effect of the r. f. field for the suppression of the end loss in the mirror field. The incident waveform to the cavity and transmitted one from the cavity are shown by the upper 2 traces. Then the transmitted waveform corresponds to the temporal change of the electric field in the cavity. The trace of I_{se} at the bottom one shows that the plasma loss at mirror end is suppressed by the r. f. field in the cavity. At the same time the plasma density increases at the mirror center as shown by the third trace, and the electron temperature does not change. The transmitted waveform does not follow the incident one, since the resonant frequency of the cavity changes with the plasma density in the cavity.

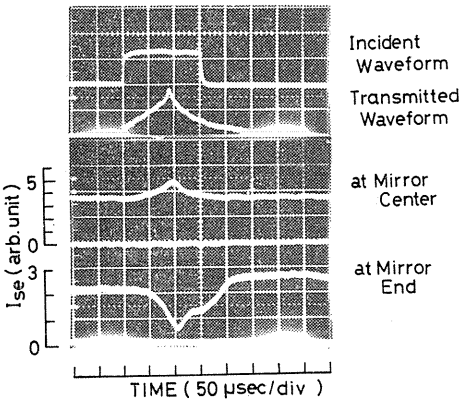

Fig. 6. 5. Temporal incident weveform to the cavity, transmitted waveform from the cavity. I_{se} at the mirror center and end.

The temporal changes of the elec-

tron saturation current I_{se} at the mirror end are shown in Fig. 6. 6 for various values of the input power P_i to the cavity. The end loss I_{se} decreases with an increase of P_i for the incident pulsed r. f. field, where the frequency is shifted only a little from the resonant frequency of the cavity.

In Fig. 6. 7 is shown the relation between the ratio-$\Delta I_{se}/I_{se0}$ and P_i, where I_{se0} is I_{se} without r. f. field and ΔI_{se} is the absolute value of the decrease of I_{se}

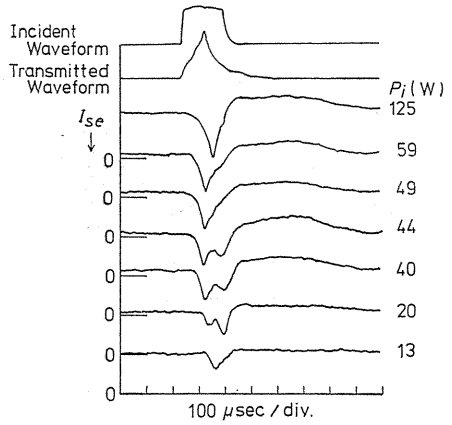

Fig. 6. 6. Incident waveform to the cavity, transmitted waveform from the cavity and I_{se} at the mirror end for the different values of P_i.

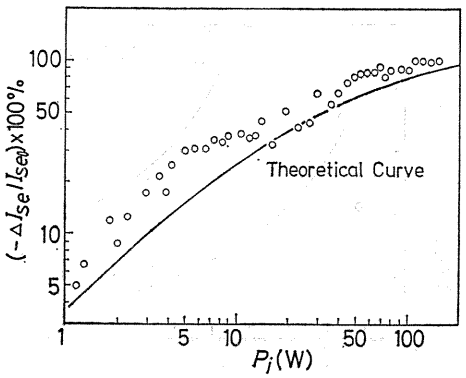

Fig. 6. 7. $-\Delta I_{se}/I_{se0}$ as a function of P_i at the mirror end.

with P_i. The 100% of the ratio means no plasma loss at the mirror end. The theoretical curve $\Delta n/n_m$, which corresponds to $\Delta I_{se}/I_{se0}$ for a constant T_e, is calculated from eq. (6. 15) by using eqs. (6. 7) (6. 13). The value of E in eq. (6. 7) is obtained from the Q-value of the cavity and the net input power to the cavity. Then the value of E is 500V/cm for the input power of 50W. The difference between the experimental values and theoretical curve would be due to the particle loss to the side wall, since the ion Larmor radius is comparable to the radius of the container.

Figure 6. 8 shows the electron temperature T_e and I_{se} at the mirror center as a function of the radial position r. The r. f. field increases the total plasma density, while the temperature T_e remains constant. This fact means the adiabatic plugging, which is expected under the experimental condition that the excursion length (0. 38mm) of electrons for E=500V/cm and the ratio (1. 5mm) of the electron thermal velocity to the frequency of r. f. field are much shorter than the characteristic

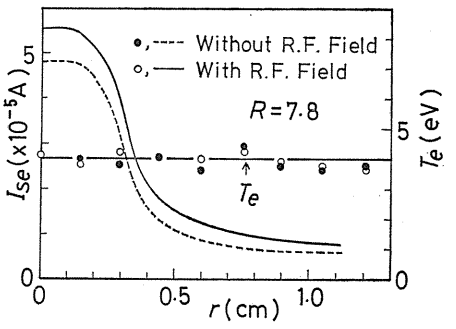

Fig. 6. 8. I_{se} and T_e as a function of r at the mirror center. P_i=70W.

length of r. f. field.

The relative increase $\Delta I_{se}/I_{se0}$ of the plasma density at the mirror center is shown in Fig. 6. 9 as a function of R. The theoretical curve is calculated from $(n-n_m)/n_m$, which is obtained from eqs. (6. 6) and (6. 14). The experimental values are one third of theoretical ones. Thus two-thirds of the particles reflected by the ponderomotive force of r. f. field are lost to the side wall.

Figure 6. 10 shows the ion saturation current I_{si} versus r measured by P 3 in the region of the uniform magnetic field, where θ is the angle between the axis of

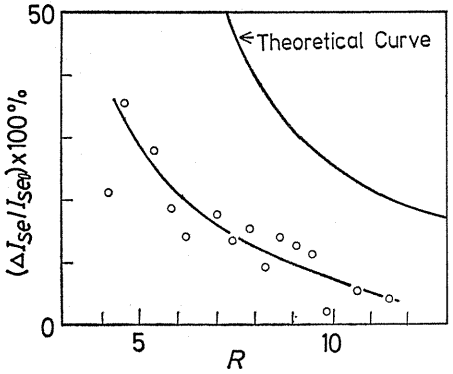

Fig. 6. 9. $\Delta I_{se}/I_{se0}$ as a function of R at the mirror center. P_i=70W.

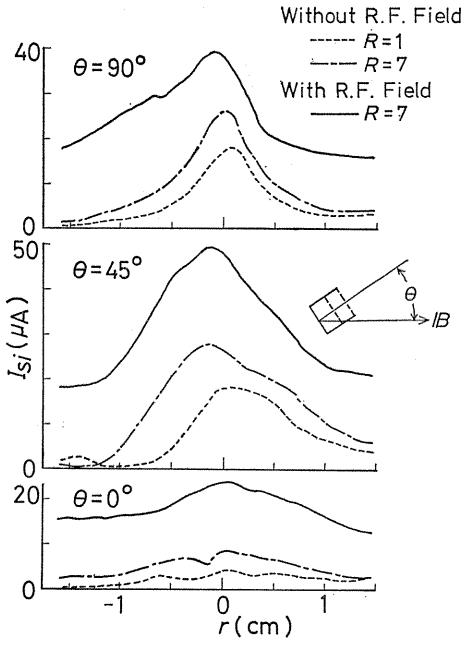

Fig. 6. 10. I_{si} as a function of r at the mirror center for the different values of R and θ. The multi-gridded probe faces to the cavity at θ=0.

the multi-gridded probe and the plasma axis as shown in the figure. The lower and medium lines show I_{si} without r. f. field at the homogeneous magnetic field (R=1) and the mirror field (R=7) respectively, and the upper lines show I_{si} increased by the r. f. field with the mirror field. Both effects of the mirror and r. f. fields are clearly demonstrated in Fig. 6. 10. However, the absolute value of the plasma density cannot be compared among the lines of the different θ, since the multi-gridded probe has not the small radius compared with the plasma one. The broadened distributions indicated by solid lines may be caused by the enhanced radial diffusion due to the r. f. field.

6. 5. Conclusion

The plasma loss is quantitatively investigated in the mirror field with and without the r. f. field.

First, the observed increase of the plasma density with the mirror ratio in the mirror center is theoretically explained.

Secondly, the suppression of the plasma loss at mirror end is observed by

applying the r. f. field with a little higher frequency than the electron plasma one. Then the adiabatic plugging without the electron and ion heating is achieved. These phenomena are theoretically explained by the ponderomotive force considering the ambipolar potential produced by the charge separation.

Thus the ponderomotive force is useful to suppress the plasma loss at the mirror end even without the cyclotron resonance. The effect of the plasma flow for the ponderomotive force and the stability as well as equilibrium for the mirror confined plasma with the end stopper should be studied as the future subjects.

7. Identification of Drift-Cyclotron Loss-Cone Instability in a Plasma and Suppression by High Frequency Field

7. 1. Introduction

Mirror machines, which have been investigated for many years as well as other machines, are said not to be hopeful as fusion reactors. One of the reasons is that an instability caused by a non-Maxwellian velocity distribution increases the radial and end loss of plasma particles.[137, 140, 141]

In order to reduce the end loss, proposals and experiments which use the high frequency or electrostatic fields have been reported by many authors.[87, 89, 93, 102, 134, 142, 143] Recently, it has been shown that the instability[104] in the mirror-confined plasma is suppressed by feeding a cold streaming plasma[114] or ionized gas.[115] However, the comparison with theory[106, 107] is not sufficient.

In this chapter is studied an instability which appears in a steady state plasma with mirror field on one side. It is reported that the instability is suppressed by a high frequency electric field near the electron plasma frequency which is applied inside a resonant cavity. The instability is identified as the drift-cyclotron loss-cone instability from the coincidence of the dispersion relation of the wave with the theoretical value predicted by Post and Rosenbluth.[106] The suppression of the instability is explained by the end stopper effect caused by the ponderomotive force.[84, 134]

In 7. 2 is described the experimental apparatus. In 7. 4, the experimental results described in 7. 3 are discussed in comparison with the theory. The obtained results are summarized in 7. 5.

7. 2. Experimental Apparatus and Procedure

Figure 7. 1 shows the schematic diagram of the apparatus. The plasma is produced by the Lisitano coil,[118] to which a microwave power is supplied from a cw magnetron operating at the frequency of 2.45 GHz with the maximum output power of 500W. The plasma has the mirror effect only on one side, as the mirror effect near the plasma production region is considered to be small becauce of scattering of particles due to the microwave field. The magnetic field strength is 330 G at the center of the apparatus.

In order to suppress the instability, the output power of cw oscillator with the maximum power of 10 W is fed to the cavity operating with TM_{010} mode through the circulator, the variable attenuator, the power meter and matching stubs. The cavity with the diameter of 30 cm and the length of 10 cm has the quality value Q of 900 and the resonant frequency of 763 MHz without plasma.

The direction of the electric field inside the cavity is parallel to the plasma axis. The electric field is picked up by a loop-antenna, and monitored on a sampling oscilloscope.

The ion temperature and ion saturation current at the center of the apparatus are measured by the multi-gridded probe P 1 with a diameter of 5mm. The plane probe P 2 with a diameter of 15 mm is utilized to measure the plasma flux in the radial direction. The instability is observed by the axially movable probe P 3 connected with the spectrum analyzer. Probe P1 is replaced by a Langmuir probe to detect the radial distribution of the instability and electron temperature, The operating pressure of He gas is 3×10^{-4} Torr, and the ion and electron temperatures are about 0.3 and 7 eV, respectively. The plasma density and Larmor radius of the ions are about 10^9 cm^{-3} and 3.4 mm, respectively. The ion-ion collision mean free path, which is shorter than the ion-neutral collision mean free path, is comparable to the machine length.

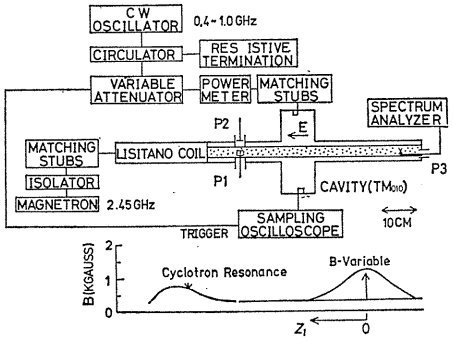

Fig. 7. 1. Schematic diagram.

In Fig. 7. 2 are shown the block diagran (a) and the arrangement of a double probe consisting of two single probes which are denoted DP 1 and DP 2 (b) to determine the wave number of the instability. The double probe is coated with the glass except the tungsten tips, and is covered by the aluminum pipes to shield the high frequency electric field. Here the two kinds of double probes with the tip separation of 5 or 2 mm are used. In Fig. 7. 2 (b), θ_1 and l are respectively the angle between the direction of the two probes and that of static magnetic field B or plasma axis, and the azimuthal distance between two probes. The DP2 can be rotated around DP 1 to change θ_1 and l. The signals of the instability from both probes are fed to the microcomputer (Iwatsu SM-1330) through the amplifiers, the bandpass-filters which pass signals from 50 kHz to 1 MHz and the analog-digital converter (Iwatsu DM-901). The auto-correlation and cross-correlation functions calculated by SM-1330 are displayed on the oscilloscope. The frequency spectra of the instability are displayed on the spectrum analyzer.

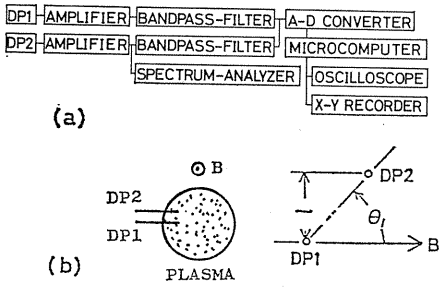

Fig. 7. 2. Block diagram (a) and double probe (b) to determine the wave number of the instability.

7. 3. *Experimental Results*

7. 3. 1. *Observation of instability*

The intensity of the light picked up by the photomultiplier in the center of apparatus is shown in Fig. 7. 3 as a function of the current I of the mirror coil

or the mirror ratio R, where R is changed by adjusting the coil current at the mirror throat. The light intensity, which is supposed to be proportional to the plasma density, starts to increase when R exceeds a small value pointed by an arrow, because the velocity distribution of the plasma produced at the resonance point is randomized by the microwave field for plasma production.

In Fig. 7. 4 are shown the frequency spectra detected by P 3 for different values of the axial distance z_1 measured from the position of the maximum magnetic field (mirror throat). An instability with the lower frequency near 50 kHz is excited not only in the mirror

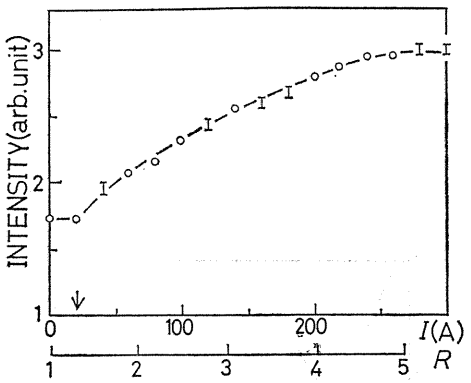

Fig. 7. 3. Light intensity at the mirror center as a function of R or I.

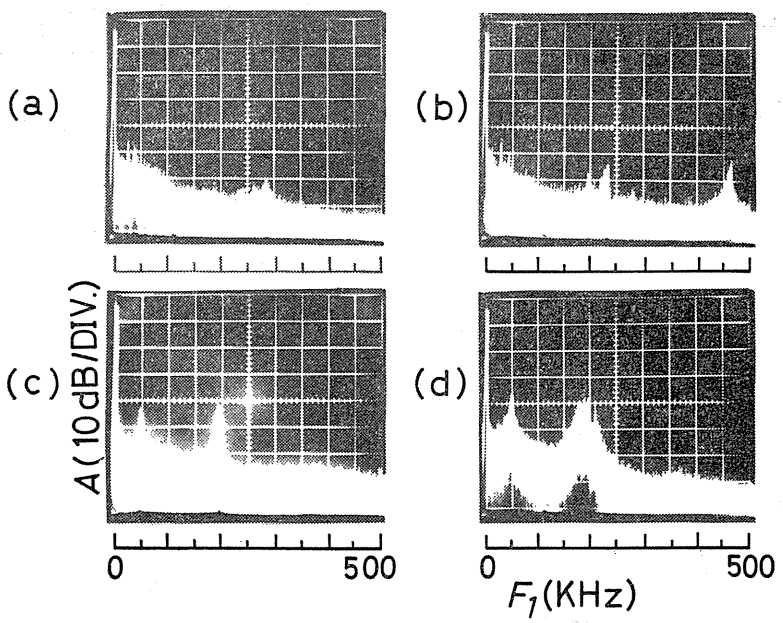

Fig. 7. 4. Frequency spectra of the instability for the different values of z_1 at $R=3$. (a) $z_1=2$ cm, (b) 6 cm, (c) 20cm, (d) 30cm.

magnetic field but also in the homogeneous field (i. e. $R=1$). Another instability with the higher frequency near 200 kHz is observed only in the mirror field (i. e. $R>1$), and its amplitude A and frequency F are shown in Fig. 7. 5 as a function of z_1.

In Fig. 7. 6 are shown A and F detected by a Langmuir probe, which is replaced by P 1, as a function of R. The lower frequency mode (a) is close to the ion cyclotron frequency of 120 kHz at $z_1=35$cm. At the mirror ratio R of 2.5 and

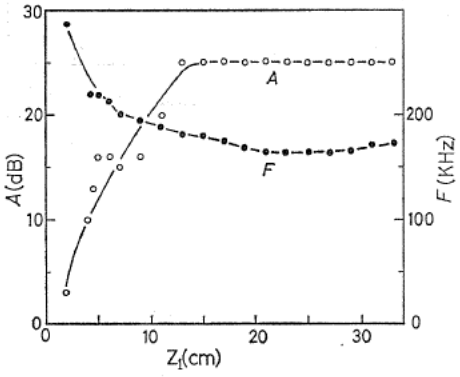

Fig. 7. 5. A and F as a function of z_1 for $R=3$.

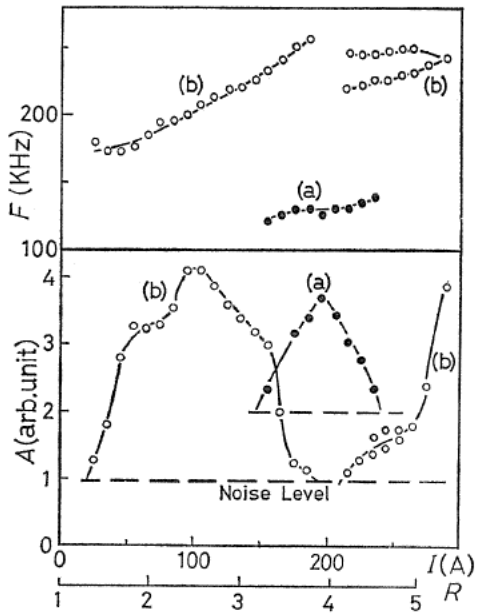

Fig. 7. 6. A and F as a function of R. (a) and (b) are respectively the lower and higher frequency modes.

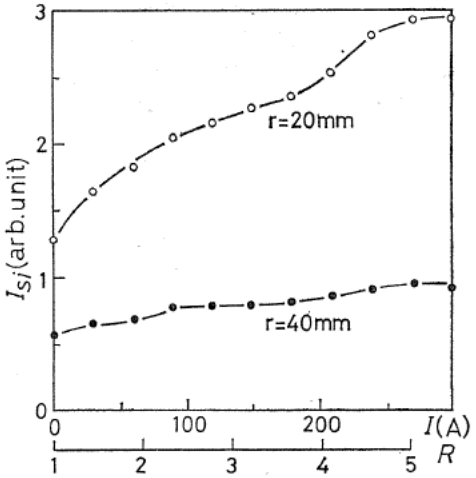

Fig. 7. 7. I_{si} of the radial diffusion flux as a function of R at the different radial positions r.

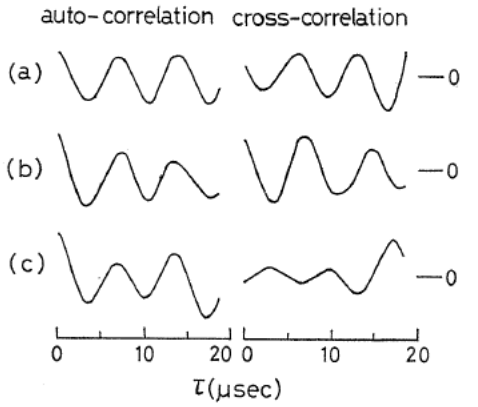

Fig. 7. 8. Auto-correlation and cross-correlation functions for the different value of θ_1 at $R=3$. (a) $\theta_1=-30°$, (b) 0°, (c) 90°.

5.5 is dominant the higher frequency mode (b), which splits into two branches for $R>4$, and the lower frequency mode grows up at $R=4$. Such instability cannot be observed in the homogeneous static magnetic field (i. e. for $R=1$).

In Fig. 7. 7 is shown the ion saturation current I_{si}, which depends on the diffusion flux, measured by P2 as a function of R, where r is the radial distance from the geometrical axis of the apparatus. The monotonous increase is due to the increase of the plasma density caused by the magnetic mirror effect. The steep increases of I_{si} for $R=1\sim2.5$ and $4\sim5$ mean the increase of the diffusion flux, and are considered to correspond to the increase of wave amplitude A, as is shown in Fig. 7. 6.

In Fig. 7. 8 are shown the auto-correlation function calculated from DP1 signal and cross-correlation function calculated from the signals of DP 1 and DP 2 with the tip separation of 5 mm for mode (a). The auto-power spectrum for the signal from DP1, which is not shown here, is also calculated by the microcomputer to determine the frequency. Figure 7. 8 (a), (b) and (c) show auto-and cross-correlation functions for θ_1 of $-30°$, $0°$, and $90°$ respectvely, where τ is the time delay. The increase of amplitude with τ in (c) is possibly due to a beating effect with the low frequency ($\sim$50 kHz) shown in Fig. 7. 4. The axial propagation of the wave is not observed in the measurement of the double probe, since there is no phase difference between two patterns in Fig. 7. 8 (b). The wave propagates in the azimuthal direction of the ion diamagnetic drift. Figure 7. 9 is obtained from several values of l, where $\Delta\tau$ is the time difference between two maxima of the auto-correlation and cross-correlation functions. The frequency F measured from the auto-power spectrum is 165 kHz, where the ion cyclotron frequency is 123 kHz. The deviation of frequency from that in Fig. 7. 6 results from a small difference of the radial density distribution.

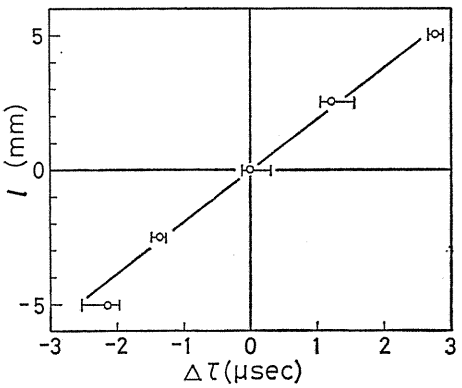

Fig. 7. 9. Relation between l and $\Delta\tau$.

The auto-correlation function $\varphi_{11}(\tau)$ and cross-correlation function $\varphi_{12}(\tau)$ for sine waves are calculated as

$$\varphi_{11}(\tau)=\frac{1}{T}\int_{-\frac{T}{2}}^{\frac{T}{2}}A^2\sin(\omega t-kx+\delta)\sin(\omega t-kx+\delta+\omega\tau)\,dt$$

$$=\frac{A^2}{2}\cos(\omega\tau), \tag{7.1}$$

$$\varphi_{12}(\tau)=\frac{1}{T}\int_{-\frac{T}{2}}^{\frac{T}{2}}A^2\sin(\omega t-kx+\delta)\sin(\omega t-kx+\delta+\omega\tau-\frac{\omega}{V_p}l)\,dt$$

$$=\frac{A^2}{2}\cos(\omega\tau-\frac{\omega}{V_p}l), \tag{7.2}$$

where T, ω, k, δ, V_p, t and x are a period, angular frequency, wave number, phase constant, phase velocity, time and distance, respectively. The phase velocity V_p and wave lenghth are calculated from $V_p=l/\Delta\tau$ and $\lambda=V_p/F$, and corrected for the $\boldsymbol{E}\times\boldsymbol{B}$ drift. By using the technique mentioned above, the wave length longer than the probe distance can be determined. The same value of V_p is obtained by the double probe with the tip separation of 2 mm.

7. 3. 2. Suppression of instability

In Fig. 7. 10 are shown the ion saturation current I_{s1}, the electron temperature T_e, the space potential Φ and the amplitude A of the wave for R of 3 as a function of r, which are measured by the Langmuir probe. In Fig. 7. 10, a and b are the amplitude A of the wave without and with the high frequency electric field of 65V/cm inside the cavity. The value of Φ is hardly affected by the high frequency field. The high frequency of 770 MHz is close to the plasma frequency.

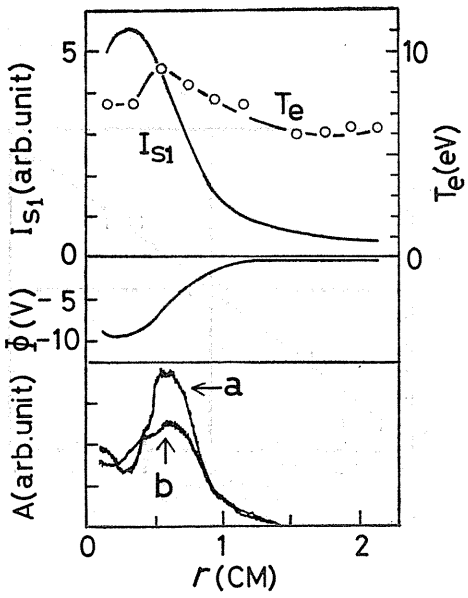

Fig. 7. 10. A, Φ, T_e and I_{s1} as a function of r. a: without high frequency field E, b: with E.

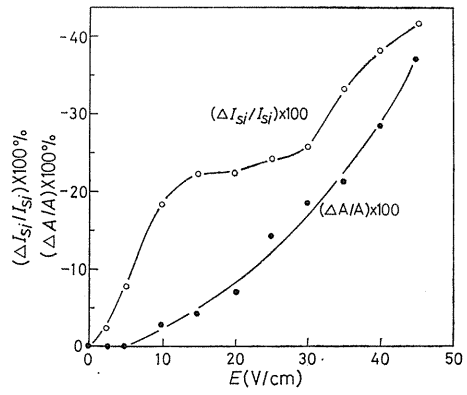

Fig. 7. 11. $\Delta A/A$ and $\Delta I_{si}/I_{si}$ of the radial diffusion flux as a function of E.

The values of $\Delta A/A$ and $\Delta I_{si}/I_{si}$ are shown in Fig. 7. 11 as a function of the high frequency electric field E, where ΔI_{si} and ΔA are the difference of A and I_{si} measured at $r=30$mm for the diffusion flux with and without the electric field. The field E can be calculated from the quality value and the net input power into the cavity. The plasma flux in the radial direction measured by P2 decreases with the wave suppression due to the high frequency electric field.

The value of $\Delta I_s/I_s$ is shown in Fig. 7. 12 as a function of R. where ΔI_s is the difference of the ion saturation current I_s measured by the multi-gridded probe P1 in the axial center for E of 50 V/cm and without E, and θ is the angle between

the axis of the multi-gridded probe and the plasma axis. The experimental value is the average one of 64 data obtained with the time interval of 0.05 sec. The values of ΔI_s in Fig. 7. 12 are related to the wave amplitude from the fact that the minimum and maximum of $\Delta I_s/I_s$ coincide with the maximum and minimum of the wave amplitude A in Fig. 7. 6 respectively.

The dependence of $\Delta I_s/I_s$ on θ in Fig. 7. 12 is shown in Fig. 7. 13 for different values of R. The increase of the plasma density near 30° is the largest.

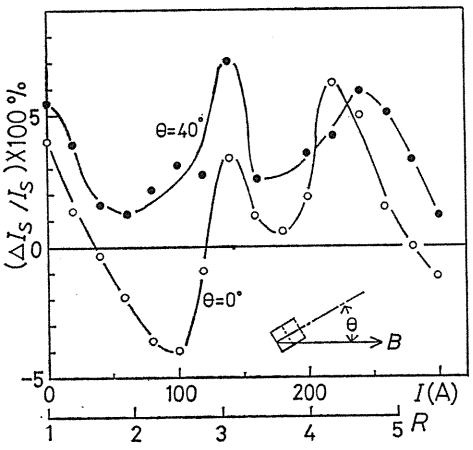

Fig. 7. 12. $\Delta I_s/I_s$ of the multi-gridded probe as a function of R for the different values of θ.

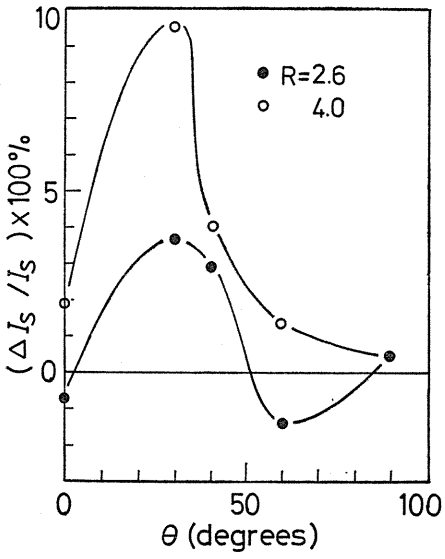

Fig. 7. 13. $\Delta I_s/I_s$ of the multi-gridded probe as a function of θ for the different values of R.

7. 4. Theoretical Consideration and Discussions

7. 4. 1. Drift-cyclotron loss-cone instability

The electrostatic instabilities in the magnetic mirror-confined plasmas were theoretically analysed by Post and Rosenbluth.[106] They predicted the wave propagating azimuthally in the direction of ion diamagnetic current. This instability is called the drift-cyclotron loss-cone (DCLC) instability, which originates from a finite radial density gradient and the loss-cone distribution.

The dispersion relation for DCLC mode is given by the following formula:

$$W^2\cot W+\beta W=\beta^{2/3}(\varepsilon\langle a_i\rangle)\pi^{4/3}\left(\frac{m}{M}+\frac{\omega_{ci}^2}{\omega_{pi}^2}\right)^{-2/3}, \tag{7.3}$$

where

$$\beta=\pi(k\langle a_i\rangle)^3\left(\frac{m}{M}+\frac{\omega_{ci}^2}{\omega_{pi}^2}\right),$$

$$\langle a_i \rangle = \left[\int \frac{f_0}{v_\perp^3} d^3v \right]^{-1/3} / \omega_{ci},$$

$$W = (\omega / \omega_{ci}) \pi,$$

$$\varepsilon = \frac{1}{N} \frac{dN}{dr},$$

and M, m, N, ω_{ci}, ω_{pi}, k, f_0, and $v_\perp$ are the ion mass, the electron mass, the plasma density, the ion cyclotron frequency, the ion plasma frequency, the wave number, the ion velocity distribution function and the perpendicular velocity of ions, respectively.

The theory[106] for the plane geometry applies to the cylindrical geometry by substituting k with J/r, where J is a mode number. The ion temperature measured by the multi-gridded probe is used for calculating the numerator of $\langle a_i \rangle$. The theoretical value of wave length λ, which is calculated from eq. (7. 3), is 1.05cm for $F=165$kHz. Since the direction of the wave propagation is the same as that of the $\boldsymbol{E}\times\boldsymbol{B}$ drift, the phase velocity in the absence of $\boldsymbol{E}\times\boldsymbol{B}$ drift should be equal to the difference between the phase velocity of 1.9×10^5cm/sec obtained from Fig. 7. 9 and the $\boldsymbol{E}\times\boldsymbol{B}$ drift speed of 3×10^4cm/sec at $r=0.65$cm. Then the phase velocity V_p and wave length λ are 1.6×10^5cm/sec and 0.97cm respectively. These results and the direction of wave propagation are in good agreements with the theoretical predictions.

7. 4. 2. Mechanism of suppression

The change of the loss-cone distribution of the plasma, which would appear in the mirror field, to the loss-hyperboloid[93] is possible by use of the ponderomotive force of the high frequency electric field. As shown in Fig. 7. 13, the number of particles pushed back by the ponderomotive force is large for θ near 30°, which is approximately equal to the critical angle $\theta_c=\sin^{-1}(1/R)^{1/2}$, and the increase of number is not observed for θ close to 90°. If the Maxwellian distribution is assumed, the $\Delta I_s/I_s$ should be flat versus θ. The observation suggests that particles reflected by both the one side mirror and ponderomotive force have the loss-hyperboloid distribution.[93] The abrupt decrease of the reflected particles for θ close to zero degree seems to represent the shadow of the multi-gridded probe. Then the suppression of DCLC instability is expected, since the free energy source to excite the instability becomes small. The suppression of the instability is observed in Figs. 7. 10 and 7. 11.

The diffusion flux in the radial direction and wave amplitude decrease with the high frequency electric field as are shown in Fig. 7. 11. This indicates that the diffusion flux is due to the wave-enhanced diffusion caused by the instability. Figure 7. 12 indicates the stopperine effect of high frequency electric field. Ionization due to the high frequency field is neglible, and the absolute value of $\Delta I_s/I_s$ is reasonable referring to the previous paper.[134] The instability affects the number of the particles reflected by the ponderomotive force, as is shown from the fact that the minimum and maximum of $\Delta I_s/I_s$ coincide with the maximum and minimum of the wave amplitude A in Fig. 7. 6.

7. 5. Conclusion

The instability, which appears at frequency comparable to the ion cyclotron

frequency in the plasma reflected by a mirror field, is identified as the drift-cyclotron loss-cone instability by comparing the experimentally determined dispersion relation with the theoretical prediction of Post and Rosenbluth[106]. The instability can be suppressed by the high frequency field. whose frequency is close to the plasma frequency.

The wave amplitude of the instability and the plasma flux in the radial direction decrease with increasing intensity of the high frequency electric field. The increase of the ion saturation current I_s to the multi-gridded probe in the mirror center depends on the angle θ between the axis of multi-gridded probe and the plasma axis. The decrease of the wave amplitude and increase of the ion saturation current are well explained by the ponderomotive force which shifts the loss-cone distribution to Maxwellian. The decrease of the plasma flux in the radial direction is also explained qualitatively as the decrease of the anomalous diffusion due to the instability.

Although the plasma is mainly reflected by only one side mirror field in the present experiment, the technique to suppress the instability by using two resonant cavities will improve the plasma confinement time in usual machines with two mirror throats.

8. Concluding Remarks

Some nonlinear interactions between the electromagnetic fields and plasmas are studied in the present thesis, and then the ponderomotive force is used to suppress the plasma loss from the mirror magnetic field and to stabilize the drift-cyclotron loss-cone (DCLC) instability. In this chapter, the results obtained in preceding chapters are summarized, and the subjects to be studied further are suggested.

In chapter 2 are described the amplification of the high frequency field and the parametric decay instability, which are produced by the high frequency electromagnetic field in the resonant cavity. When the frequency of the electromagnetic wave is slightly higher than the maximum electron plasma frequency, the decrease of the quality factor Q and increase of the electron temperature begin to be observed at a certain input power to the cavity. This power agrees with the theoretical threshold value of the decay instability for the homogeneous plasma. Then the ion acoustic and electron plasma waves begin to be observed when the input power is somewhat higher than the threshold value for the homogeneous plasma. This second threshold power is found to correspond to the threshold of the decay instability in the inhomogeneous plasma. When the frequency of the electromagnetic wave is lower than the maximum electron plasma frequency, the amplification of the high frequency electric field and decrease of the density are observed at the cut-off region. This decrease of the density is explained in terms of the ponderomotive force by the amplified electric field.

In chapter 3 is experimentally confirmed the theory of the double resonance parametric instability by using the two electromagnetic waves with the frequency difference which is twice the ion acoustic wave frequency. The parametric decay instability excited by the two pump fields has a lower threshold and larger growth rate than that excited by one pump field. The ratio of the threshold for two pumps to that for one pump nearly agrees with the theory. The slight difference

between the theory and experiment will be due to the inhomogeneity of the plasma used in the experiment.

In chapter 4 is described the modulational instability of the electron plasma wave excited by a resonant cavity. The modulational and parametric instabilities are experimentally distinguished by the control of the plasma density. The modulational wave of the electron plasma wave grows and then damps spatially, and the frequency and amplitude of the modulational wave are respectively proportional to the electric field of the electron plasma wave and to its square. These obtained results are in agreement with the theoretical prediction based on coupling of the nonlinear Schrödinger equation with the equation of the ion acoustic wave including the term of the ponderomotive force. Then the low frequency fluctuation of the ion density with the phase difference of π to the envelope of the electron plasma wave is produced with increasing the amplitude of the electron plasma wave. This phenomenon is explained by the ion acoustic wave excited by the ponderomotive force due to the modulated electron plasma wave.

In chapter 5, the ponderomotive force is quantitatively confirmed by the high frequency electric field in the resonant cavity. The increase of the density and no change of the electron temperature are observed in the upstream side of the plasma. On the other hand, the decrease of the density and increase of the temperature are observed in the downstream side of the plasma. The relation between the density decrease and the high frequency electric field is in agreement with theory including the ponderomotive force due to the electric field smaller than a certain value. The instability excited with the higher electric field decreases the density in the downstream side.

In chapter 6, the ponderomotive force is utilized to suppress the plasma loss from the mirror magnetic field. The plasma density at the mirror center increases with the mirror ratio due to the mirror effect. When the electromagnetic field is applied to the plasma, the plasma density at the mirror center increases, and the plasma loss from the mirror magnetic field decreases. Then the adiabatic plugging without the electron and ion heatings is achieved. These phenomena are explained by the mirror effect with ponderomotive force.

In chapter 7 are described the identification and stabilization of DCLC instability. The observed wave with about the ion cyclotron frequency localizes in the radial region with the sharp density gradient, and propagates in the direction of the ion diamagnetic current. These characteristics and the dispersion of wave are in good agreement with the theory of DCLC instability. The DCLC instability is next stabilized by the introduction of the ponderomotive force, which shifts the loss-cone velocity distribution to the loss-hyperboloid one.

Finally, the some subjects left in the future are mentioned below on the parametric, modulational instabilities and ponderomotive force studied in this thesis. The saturated state of the parametric instability in the inhomogeneous plasms must be studied for further understanding of the laser plasma interaction and for the application to the plasma heating Then the efficiency of the double resonance parametric instability for the plasma heating needs to be investigated by using two electromagnetic waves with the higher power. Next, the developed phenomena of the modulational instability must be theoretically studied including the generation of the magnetic field reported in the recent laser experiment. The future subjects on the ponderomotive force will be to consider the influence of the plasma flow, and to investigate the influence of the ponderomotive force on the stability and

equilibrium for the mirror-confined plasma with the end stopper. Moreover, the discovery and research of the new nonlinear phenomena are important for the development of the plasma physics and the realization of the nuclear fusion reactor.

Acknowledgements

The authors would like to express their appreciation to Professor Takashige Tsukishima and Dr. Hedeo Sugai for their helpful advice and critical reading of the manuscript. The authors also wish to thank Professor Takayoshi Okuda and Professor Shigeki Miyajima of Nagoya University for their helpful suggestion. Moreover, the authors wish to thank Professor Kazuo Minami of Tokyo Institute of Technology, Professor Masashi Kando of Shizuoka University, Dr. Kazuyuki Ohe of Nagoya Institute of Technology, Dr. Tatsuki Ogino of Research Institute of Atmospherics and Dr. Tadatsugu Hatori of Institute of Plasma Physics of Nagoya University for their valuable discussions and useful suggestions.

One of the authors is indebted to Professor Masanori Hara of Kyushu University for drawing his attention to the plasma physics. Thanks are due to Mr Shun-ichi Hirose, Mr. Tomohiko Yamada and Mr. Osamu Matumoto for their assistance and discussions. The authors also wish to thank Mr. Mitsuo Mori for the glass work, and Miss Naoko Yanagisawa for fine typing of the manuscript.

References

1) L. Spitzer, Jr.: Physics of Fully Ionized Gases (1956) Interscience Publishers, New York.
2) T. H. Stix: The Theory of Plasma Waves (1962) McGraw-Hill, New York.
3) M. A. Leontovich: Reviews of Plasma Physics, Vol. 3 (1967) Consultants Bureau, New York.
4) A. B. Mikhailovskii: Theory of Plasma Instabilities, Vol. 1 and 2 (1974) Consultants Bureau, New York - London.
5) A. I. Akhiezer, I. A. Akhiezer, R. V. Polovin, A. G. Sitenko and K. N. Stepanov: Plasma Electrodynamics, Vol. 1 (1975) Pergamon Press, New York.
6) M. A. Heald and C. B. Wharton: Plasma Diagnostics with Microwaves (1965) John & Sons, New York - London - Sydney.
7) V. P. Silin: Soviet Physics-JETP **21** (1965) 1127.
8) D. F. DuBois and M. V. Goldman: Phys. Rev. Letters **14** (1965) 544.
9) M. V. Goldman and D. F. DuBois: Phys. of Fluids 8 (1965) 1404.
10) E. A. Jackson: Phys. Rev. **153** (1967) 235.
11) K. Nishikawa: J. Phys. Soc. Japan **24** (1968) 916, 1152.
12) Y. C. Lee and C. H. Su: Phys. Rev. **152** (1966) 129.
13) D. F. DuBois and M. V. Goldman: Phys. Rev. **164** (1967) 207.
14) P. Kaw, E. Valeo and J. M. Dawson: Phys. Rev. Letters **25** (1970) 430.
15) J. R. Sanmartin: Phys. of Fluids **13** (1970) 1533.
16) V. V. Pustovalov and V. P. Silin: Soviet Physics-JETP **32** (1971) 1198.
17) A. A. Galeev, V. N. Oraevskii and R. Z. Sagdeev: ZHETF Pis. Red. **16** (1972) 194.
18) G. V. Hoven and D. A. Phelps: Phys. of Fluids **16** (1973) 495.
19) A. A. Galeev and R. Z. Sagdeev: Nuclear Fusion **13** (1973) 603.
20) N. E. Andreev and V. P. Silin: Soviet Physics-JETP **41** (1975) 253.

21) F. W. Perkins and J. Flick: Phys. of Fluids **14** (1971) 2012.
22) A. Takeo: J. Phys. Soc. Japan **22** (1967) 1282.
23) T. Amano and M. Okamoto: J. Phys. Soc. Japan **26** (1969) 529.
24) M. N. Resenbluth: Phys. Rev. Letters **29** (1972) 565.
25) R. B. White, C. S. Liu and M. N. Resenbluth: Phys. Rev. Letters **31** (1973) 520.
26) D. Pesme, G. Laval and R. Pellat: Phys. Rev. Letters **31** (1973) 203.
27) D. R. Nicholson and A. N. Kaufman: Phys. Rev. Letters **33** (1974) 1207.
28) Y. C. Lee and P. K. Kaw: Phys. Rev. Letters **28** (1974) 135.
29) D. F. DuBois, D. W. Forslund and E. A. Williiams: Phys. Rev. Letters **33** (1974) 1013.
30) V. P. Silin and A. N. Starodub: Soviet Physics-JETP **39** (1974) 82.
31) D. Arnush, K. Nishikawa, B. D. Fried, C. F. Kennel and A. Y. Wong: Phys. of Fluids **16** (1973) 2270.
32) T. Tanaka: J. Phys. Soc. Japan **42** (1977) 670.
33) J. J. Thomson and Jack I. Karush: Phys. of Fluids **17** (1974) 1608.
34) D. F. DuBois and M. V. Goldman: Phys. Rev. Letters **28** (1972) 218.
35) B. Bezzerides and D. F. DuBois: Phys. Rev. Letters **36** (1976) 729.
36) S. Y. Yuen: Phys. of Fluids **18** (1975) 1308.
37) E. Valeo, C. Oberman and F. W. Perkins: Phys. Rev. Letters **28** (1972) 340.
38) B. B. Godfrey, K. A. Taggart and C. E. Rhoades, Jr.: Phys. of Fluids **16** (1973) 2279.
39) V. V. Pustovalov, V. P. Silin and V. T. Tikhonchuk: Soviet Physics-JETP **39** (1974) 452.
40) R. A. Stern and N. Tzoar: Phys. Rev. Letters **17** (1966) 903.
41) H. Dreicer, D. B. Henderson and J. C. Ingraham: Phys. Rev. Letters **28** (1971) 1616.
42) H. W. Hendel and J. T. Flick: Phys. Rev. Letters **31** (1973) 199.
43) H. P. Eubank: Phys. of Fluids **14** (1971) 2551.
44) R. Stenzel and A. Y. Wong: Phys. Rev. Letters **28** (1972) 274.
45) K. Mizuno and J. S. Degroot: Phys. Rev. Letters **35** (1975) 219.
46) I. R. Gekker and O. V. Sizukhin: Soviet Physics-JETP Letters **9** (1969) 243.
47) D. Phelps, N. Rynn and G. V. Hoven: Phys. Rev. Letters **26** (1971) 688.
48) R. N. Franklin, S. M. Hamberber, G. Lampis and G. J. Smith: Phys. Rev. Letters **27** (1971) 1119.
49) T. K. Chu and H. W. Hendel: Phys. Rev. Letters **29** (1972) 634.
50) D. W. Stowe and H. Böhmer: Phys. of Fluids **16** (1973) 2247.
51) J. H. Brownell, H. Dreicer, R. F. Ellis and J. C. Ingraham: Phys. Rev. Letters **33** (1974) 1210.
52) M. Porkolab: Proc. 12th Int. Conf. Ioniz. Phenom. Gases, Eindhoven **2** (1975) p. 86.
53) S. Hiroe and H. Ikegami: Phys. Rev. Letters **19** (1967) 1414.
54) R. P. H. Chang and M. Porkolab: Phys. Rev. Letters **31** (1973) 1241.
55) K. Yatsui and T. Imai: Phys. Rev. Letters **35** (1975) 1279.
56) S. P. Obenschain, N. C. Luhmann, Jr. and P. T. Greiling: Phys. Rev. Letters **36** (1976) 1309.
57) M. Porkolab, S. Bernabei, W. M. Hooke, R. W. Motley and T. Nagashima: Phys. Rev. Letters **38** (1977) 230.
58) B. Grek and M. Porkolab: Phys. Rev. Letters **30** (1973) 836.
59) M. Okabayashi, K. Chen and M. Porkolab: Phys. Rev. Letters **31** (1973) 1113.
60) L. I. Grigoreva: Soviet Physics-JETP **33** (1971) 329.
61) V. L. Vdovin: Soviet Physics-JETP Letters **14** (1971) 149.
62) T. Taniuti and N. Yajima: J. Math. Phys. **10** (1969) 1369.
63) T. Taniuti and C. C. Wei: J. Phys. Soc. Japan **24** (1968) 941.
64) T. Taniuti and H. Washimi: Phys. Rev. Letters **21** (1968) 209.
65) V. I. Karpman and E. M. Krushkal: Soviet Physics-JETP **28** (1968) 277.
66) N. Asano, T. Taniuti and N. Yajima: J. Math. Phys. **10** (1969) 2020.
67) K. Simizu and Y. H. Ichikawa: J. Phys. Soc. Japan **33** (1972) 789.
68) A. Hasegawa: Phys. of Fluids **15** (1972) 870.

69) M. Kako: J. Phys. Soc. Japan **33** (1972) 1678.
70) V. E. Zakharov: Soviet Physics-JETP **35** (1972) 908.
71) K. Nishikawa, H. Hojo, K. Mima and H. Ikezi: Phys. Rev. Letters **33** (1974) 148.
72) P. K. Kaw and K. Nishikawa: J. Phys. Soc. Japan **38** (1975) 1753.
73) K. Mio, T. Ogino, K. Minami and S. Takeda: J. Phys. Soc. Japan **41** (1976) 667.
74) H. C. Kim, R. L. Stenzel and A. Y. Wong: Phys. Rev. Letters **33** (1974) 886.
75) H. Ikezi, K. Nishikawa and K. Mima: J. Phys. Soc. Japan **37** (1974) 766.
76) B. H. Quon, A. Y. Wong and B. H. Ripin: Phys. Rev. Letters **32** (1974) 406.
77) A. Y. Wong and B. H. Quon: Phys. Rev. Letters **34** (1975) 1499.
78) A. Y. Wong and R. L. Stenzel: Phys. Rev. Letters **34** (1975) 727.
79) H. Ikezi, R. P. H. Chang and R. A. Stern: Phys. Rev. Letters **36** (1976) 1047.
80) E. Valeo anb W. Kruer: Phys. Rev. Letters **33** (1974) 750.
81) K. Estabrook, E. Valeo and W. Kruer: Phys. Lett. **49A** (1974) 109.
82) G. J. Morales and Y. C. Lee: Phys. Rev. Letters **33** (1974) 1016.
83) G. J. Morales and Y. C. Lee: Phys. of Fluids **19** (1976) 690.
84) A. V. Gurevich and L. P. Pitaevskii: Soviet Physics-JETP **18** (1964) 855.
85) R. Klima: Soviet Physics-JETP **23** (1966) 534.
86) M. E. Marhic: Phys. of Fluids **18** (1975) 837.
87) V. I. Veksler: Proceedings of the CERN Symposium on High Energy Accelerators Pion Physics, Geneva (1956) p. 80.
88) A. V. Gaponov and M. A. Miller: Soviet Physics-JETP **7** (1958) 168.
89) T. Consoli: Phys. Letters **7** (1963) 254.
90) C. J. H. Watson and L. G. Kuo-Petravic: Phys. Rev. Letters **20** (1968) 1231.
91) F. Werkoff: Plasma Phys. **14** (1972) 897.
92) A. J. Hatch and J. L. Shohet: Phys. of Fluids **17** (1974) 232.
93) B. B. Mcharg, Jr. and M. E. Oakes: Phys. of Fluids **18** (1975) 1059.
94) T. J. Dolan, B. L. Stansfield and J. M. Larsen: Phys. of Fluids **18** (1975) 1383.
95) C. H. Woods: Phys. of Fluids **20** (1977) 252.
96) S. A. Self and H. A. H. Boot: J. Electron. Control **6** (1959) 527.
97) R. Bardet, T. Consoli and R. Geller: Nuclear Fusion **5** (1965) 7.
98) T. Sato, S. Miyake, T. Watari, Y. Kubota and K. Takayama: J. Phys. Soc. Japan **28** (1970) 808.
99) C. D. Johnson: J. Appl. Phys. **44** (1973) 1581.
100) S. Hiroe, T. Sato, T. Watari, S. Hidekuma, R. Kumazawa, K. Adati, T. Shoji, S. Kawasaki, A. Miyahara, K. Akaishi, Y. Kubota, N. Watanabe and S. Miyake: Phys. of Fluids **21** (1978) 676.
101) T. Watari, S. Hiroe and T. Sato: Phys. of Fluids **17** (1974) 2107.
102) V. D. Douger-Jabon, K. S. Golvanivsky and V. I. Karyaka: 7th Europ. Conf. on Contr. Fusion and Plasma Physics, Lausanne, Vol. 1 (1975) p. 33.
103) C. F. Shelby and A. J. Hatch: Phys. Rev. Letters **29** (1972) 834.
104) T. C. Simonen: Phys. of Fluids **19** (1976) 1365.
105) W. C. Turner, E. J. Powers and T. C. Simonen: Phys. Rev. Letters **39** (1977) 1088.
106) R. F. Post and M. N. Rosenbluth: Phys. of Fluids **9** (1966) 730.
107) Y. Shima and T. K. Fowler: Phys. of Fluids 8 (1965) 2245.
108) W. M. Tang, L. D. Pearlstein and H. L. Berk: Phys. of Fluids **15** (1972) 1153.
109) D. E. Baldwin, H. L. Berk and L. D. Pearlstein: Phys. Rev. Letters **36** (1976) 1051.
110) R. E. Aamodt: Phys. of Fluids **20** (1977) 960.
111) R. C. Davidson and N. T. Gladd: Phys. of Fluids **20** (1977) 1516.
112) R. E. Aamodt, Y. C. Lee, C. S. Liu and M. N. Rosenbluth: Phys. Rev. Letters **39** (1977) 1660.
113) A. Hasegawa: Phys. Rev. Letters **40** (1978) 938.
114) F. H. Coensgen, W. F. Cummins, B. G. Logan, A. W. Molvik, W. E.Nexsen, T. C. Simonen, B. W. Stallard and W. C. Turner: Phys. Rev. Letters **35** (1975) 1501.
115) B. G. Logan, J. F. Clauser, F. H. Coensgen, D. L. Correl, W. F. Cummins, C. Gorma-

zano, A. W. Molvik, W. E. Nexsen, T. C. Simonen, B. W. Sallard and W. C. Turner: Phys. Rev. Letters **37** (1976) 1468.
116) B. I. Kanaev, V. P. Pastukhov and E. E. Yushmanov: Soviet Physics-JETP Letters **18** (1973) 204.
117) V. V. Arsenin and V. P. Pastukhov: Sov. J. Plasma Phys. **3** (1977) 172.
118) G. Lisitano: Proc. 7th Int. Conf. Ioniz. Phenom. Gases. Beograd, Vol. 1 (1966) p. 464.
119) G. Lisitano, R. A. Ellis, Jr., W. M. Hooke and T. H. Stix: Rev. Sci. Inst. **39** (1968) 295.
120) R. B. White and F. F. Chen: Plasma Phys. **16** (1974) 565.
121) V. P. Milantiev and V. A. Tourikov: 7th Europ. Conf. on Centr. Fusion and Plasma Physics, Lausanne, Vol. 1 (1975) p. 35.
122) M. Porkolab, V. Arunasalam and R. A. Ellis, Jr.: Phys. Rev. Letters **29** (1972) 1438.
123) R. P. H. Chang and M. Porkolab: Phys. Rev. Letters **32** (1974) 1227.
124) W. L. Kruer, P. K. Kaw, J. M. Dawson and C. Obermann: Phys. Rev. Letters **24** (1970) 987.
125) J. J. Thomson, R. J. Fael and W. L. Kruer: Phys. Rev. Letters **31** (1973) 918.
126) T. Ogino and S. Takeda: J. Phys. Soc. Japan **38** (1975) 1133.
127) K. Minami, K. P. Singh, M. Masuda and K. Ishii: Phys. Rev. Letters **33** (1974) 740.
128) H. Sugai, M. Maruyama, M. Sato and S. Takeda: Phys. Letters **64A** (1977) 295.
129) B. Agdur and B. Enander: J. Appl. Physics **33** (1962) 575.
130) A. Mase and T. Tsukishima: Phys. of Fluids **18** (1975) 464.
131) H. Akiyama, M. Kando, K. Minami and S. Takeda: J. Phys. Soc. Japan **40** (1976) 839.
132) S. C. Brown: Proc. 2nd Intl. Conf. Peaceful Uses of Atomic Energy, Geneva **32** (1958) 394.
133) H. Akiyama, S. Hirose and S. Takeda: J. Phys. Soc. Japan **42** (1977) 1715.
134) H. Akiyama and S. Takeda: J. Phys. Soc. Japan **41** (1976) 1036.
135) K. Mima, K. Nishikawa and H. Ikezi: Phys. Rev. Letters **35** (1975) 726.
136) T. K. Fowler: Nuclear Fusion **9** (1969) 3.
137) M. S. Ioffe and B. B. Kadomtsev: Soviet Physics-Uspekhi **13** (1970) 225.
138) G. G. Kelley: Plasma Phys. **9** (1967) 503.
139) H. Akiyama and S. Takeda: J. Phys. Soc. Japan **43** (1977) 1739.
140) Yu. V. Gott, M. S. Ioffe and V. G. Tel'kovskii: Nuclear Fusion, Suppl. Part Ⅲ (1962) 1045.
141) R. W. Moir and R. F. Post: Nuclear Fusion **9** (1969) 253.
142) A. A. Ware and J. E. Faulkner: Nuclear Fusion **9** (1969) 353.
143) S. Hiroe, S. Hidekuma, T, Watari, T. Shoji, T. Sato and K. Takayama: Nuclear Fusion **15** (1975) 769.